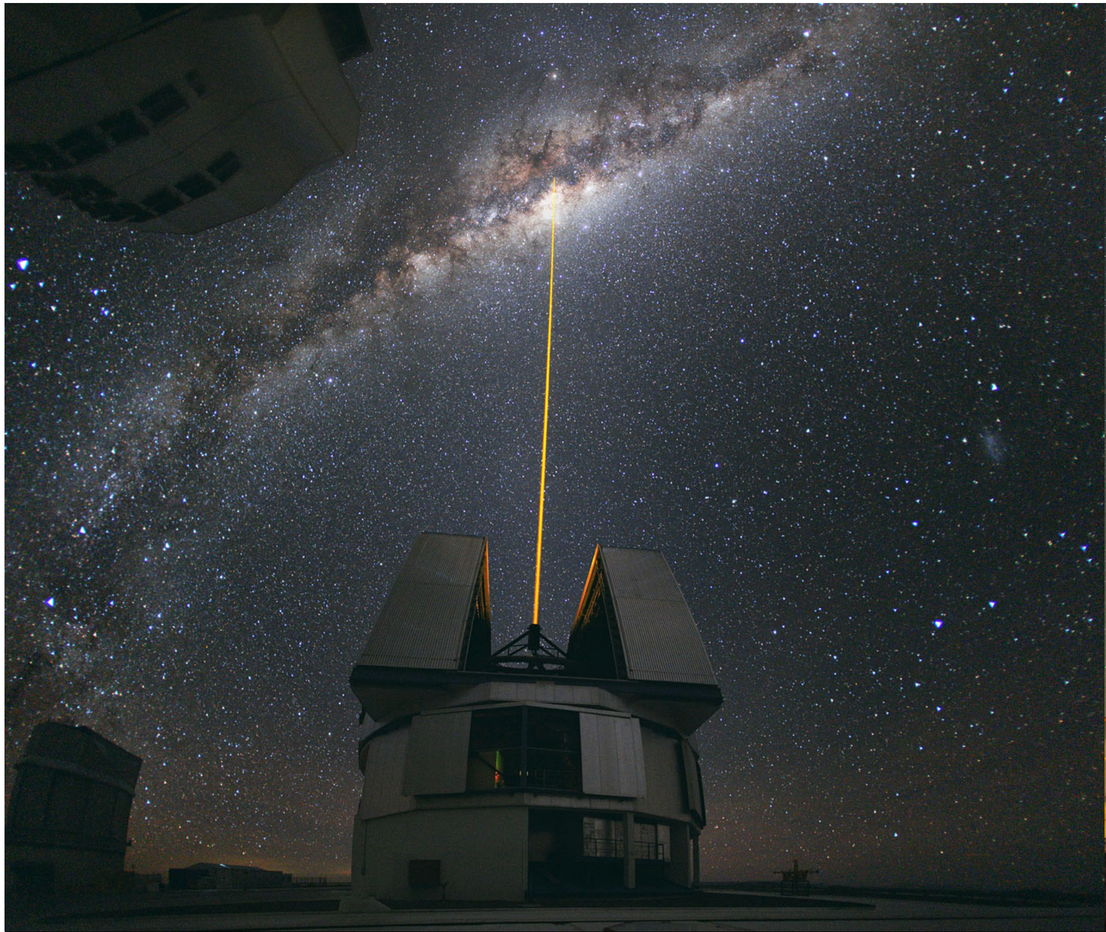

Using SgrA* to test Theories of Gravity

Mariafelicia De Laurentis

University of Naples Federico II

Event Horizon Telescope

INFN NAPOLI

FLAG-Meeting 2024 (Catania)

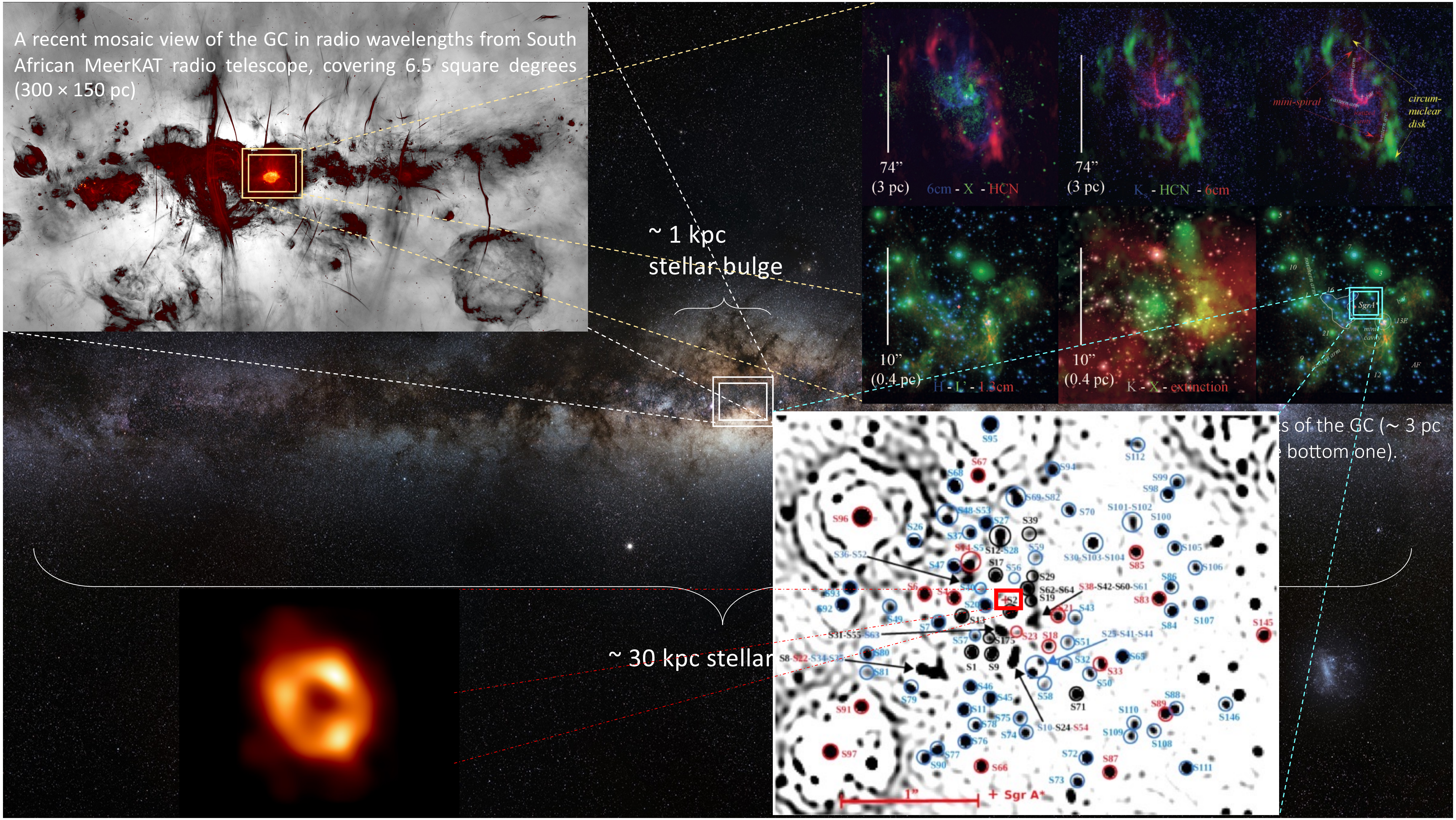
A recent mosaic view of the GC in radio wavelengths from South African MeerKAT radio telescope, covering 6.5 square degrees (300 × 150 pc)
~ 1 kpc stellar bulge
74”
(3 pc)
6cm - X - HCN
74”
(3 pc)
K - HCN - 6cm
mini-spiral
circum-nuclear disk
10”
(0.4 pc)
H - L’ - 1.3cm
10”
(0.4 pc)
K - X - extinction
SgrA*
s of the GC (~ 3 pc
bottom one).
~ 30 kpc stellar
1”
+ Sgr A*

A supermassive object in the Galactic Center

Andrea Ghez

2020 Nobel Prize on Physiscs

Reinhard Genzel

Stars orbiting around Sgr A* have been detected and monitored:

- They move with large velocities in Keplerian orbits, about ~ 10.000 km/s
- These orbits jointly determine the mass and distance to Sgr A* to high precision, particularly the ratio M/D that determines the angular size of the black hole on the sky

$M \sim 4 \times 10^6 M_\odot$ | $D \sim 8Kpc$ | $\theta \sim 50\mu as$

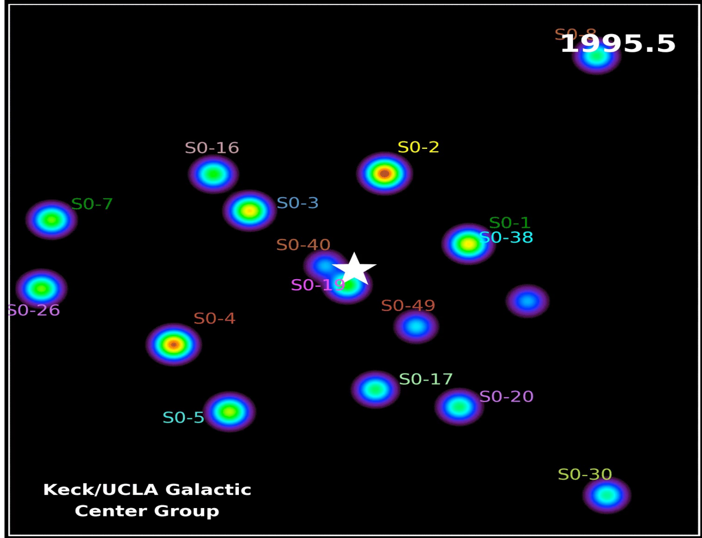

Compatible with a SMBH as described by General Relativity

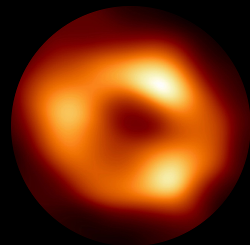

EHTC *et al* 2022
ApJL **930** L12 - L17

Schödel et al. 2002; Ghez et al.2003, 2008; Gillessen et al. 2009; Gravity Collaboration et al. 2018a; Do et al. 2019; Gravity Collaboration et al. 2019; Bower, G. C. et al., Science, 2004, 304, 704-708

First step: testing SgrA* space-time at large distances

S2-star the main actress

- Apparent 2.2 μ m (NIR K -band) magnitude of m_K= 14
- Orbital period P≈ 16 yr
- Semimajor axis a=125mas (or ~10^3 AU at an 8 kpc distance);
- Eccentricity e ~0.88
- Slowly rotating, single, main-sequence B-star of age ≈ 6 Myr

Its orbit provided some of the best evidence for the existence of a black hole.

May 19, 2018 passed pericentre at 120 AU (≈1400 R_S) with an orbital speed of 7700 km s^{-1}

Astrometric and spectroscopic data allowed to test the strong gravitational field of a massive black hole and the detection of (for the first time on S2!):

The gravitational redshift
Star close to SgrA*

The transverse Doppler effect
Star fast at pericenter

The orbital precession
General relativistic effect

$$\Delta\phi^{\mathrm{PPN1_{SP}}}_{\mathrm{per\,orbit}} = f_{\mathrm{SP}} \frac{3\pi R_S}{a(1-e^2)} \overset{\mathrm{for\,S2}}{=} f_{\mathrm{SP}} \times 12.1'$$

GRAVITY Collaboration 2017, A&A, 602, 23 ;2018a, A&A, 615, 15G ;2020, A&A, 636, L5

Its best-fit value is f_{SP} = 1.10 ± 0.19 where f_{SP} =1 leads to GR, and f_{SP} =0 reduces to Newtonian theory.

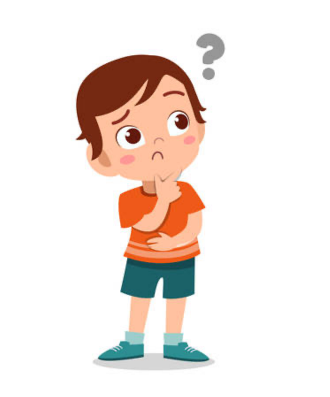

Some questions (I)

Preamble:

The analysis of Keck and GRAVITY/VLTI is performed in the so-called weak field regime.

Question:

What happens if we find another star much closer to SgrA*?
Is it still possible to use the weak field approach?

Answer: No

Solution:

Adopt a fully relativistic description

Some questions (II)

Preamble:

The mathematical description of astrophysical BHs is based on solutions to the Einstein field equations and therefore founded on GR.

There also exist many BH solutions in extended/alternative/modified theories of gravity, and to date, observational constraints, most notably in the strong-field regime, are lacking.

Question:

- Is General Relativity the ultimate theory of gravity? What do we mean by a good theory of gravity? Do we need a new theory of gravity?
- Can we quantify deviations on the metric parameters of non-GR spacetimes?
- Can we quantify deviations from the classical black hole metrics in GR?
- Can we argue something about the nature of dark matter?

Let's start with question II

Theories of Gravity

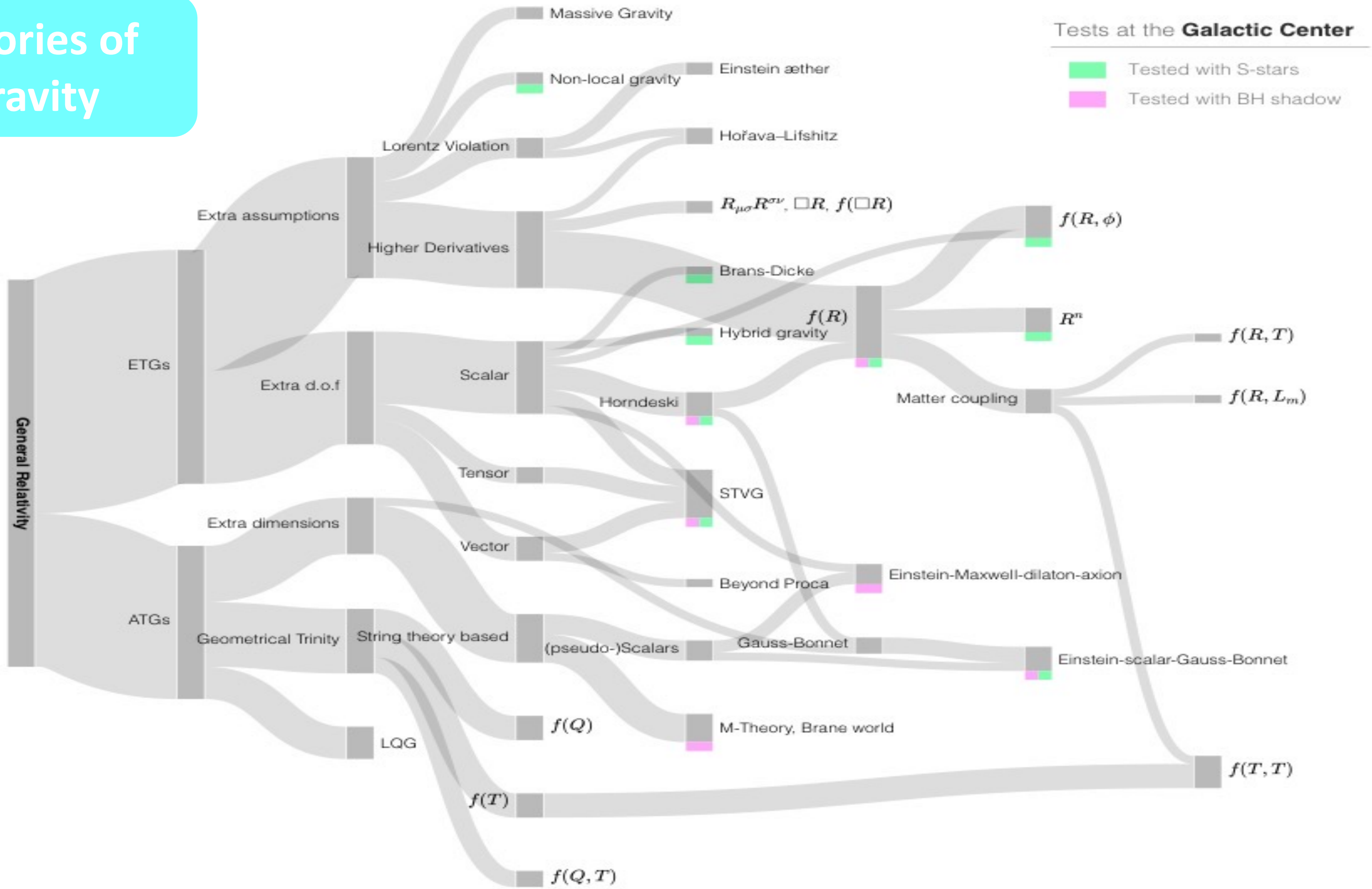

De Laurentis, M., De Martino, I., Della Monica, R. Rep. Prog. Phys. 86 104901 (2023)(INVITED REVIEW)

Let's go back to the answer to the first question

Testing alternatives to the Schwarzschild BH: some examples

f(R)- theory

Horndeski Theory

MOG (Modified Gravity)/ STVG (Scalar Tensor Vector Gravity)

- Shaymatov S., Ahmedov B., De Laurentis M. et al., ApJ 2023, 959, 6
- Fernández R., Della Monica R., de Martino I. 2023, arXiv:2306.06937
- Della Monica R., de Martino I. 2023, arXiv:2305.10242
- Della Monica R., de Martino, I., De Laurentis M. 2023, MNRAS, 521, 474
- Della Monica R., de Martino I. 2023, A&A, 670, L4.
- Cadoni M., De Laurentis M., De Martino I., et al. 2023, PRD, 107, 044038
- Della Monica R., de Martino I., Vernieri D., et al. 2023, MNRAS, 519, 1981.
- De Laurentis M., De Martino I., Della Monica R. Rep. Prog. Phys. 86 104901 (2023)(**INVITED REVIEW)**
- Della Monica R., de Martino I., De Laurentis, M. 2022, MNRAS, 510, 4757.
- Della Monica R. & de Martino I. 2022, JCAP, 2022, 007.
- Della Monica R., de Martino I., De Laurentis M. 2022, Universe, 8, 137
- D'Addio A., Casadio R., Giusti A., De Laurentis M. 2022 Phys.Rev.D 105, 10, 104010
- De Martino I., della Monica R., De Laurentis M. 2021, PRD, 104, L101502
- De Laurentis M., De Martino I., Lazkoz R. 2018, European Physical Journal C, 78, 916
- De Laurentis M., De Martino I., Lazkoz R. 2018, PRD, 97, 104068
- De Martino I., Lazkoz R., De Laurentis M. 2018, PRD, 97, 104067
- De Laurentis M., Younsi, Z., Porth O., Mizuno Y., & Rezzolla 2018 L. Phys. Rev. D 97, 104024

New methodology: a fully relativistic approach

Fully relativistic equations of motion for massive particles can be obtained from the geodesic equations for time-like geodesics of the spherically symmetric metric:

$$\frac{d^2x^\mu}{ds^2} + \Gamma^\mu_{\nu\rho}\frac{dx^\nu}{ds}\frac{dx^\rho}{ds} = 0$$

These equations provide differential equations for the four space-time

$$\{t(s), r(s), \theta(s), \phi(s)\}$$

Affine parameter

$$ds^2 = g_{tt}(r; M, \alpha \ldots)dt^2 + g_{rr}(r; M, \alpha \ldots)dr^2 + r^2 d\Omega^2$$

Aerial radius

Central mass

One or more additional parameters

Depending on the specific model

For example, Schwarzschild

$$g_{tt} = \left(1 - \frac{2M}{r}\right)$$

$$g_{rr} = \left(1 - \frac{2M}{r}\right)^{-1}$$

New methodology: a fully relativistic approach

Fully relativistic equations of motion for massive particles can be obtained from the geodesic equations for time-like geodesics of the spherically symmetric metric:

$$\frac{d^2x^\mu}{ds^2} + \Gamma^\mu_{\nu\rho}\frac{dx^\nu}{ds}\frac{dx^\rho}{ds} = 0$$

These equations provide differential equations for the 4D space-time

$$\{t(s), r(s), \theta(s), \phi(s)\}$$

Affine parameter

Initial conditions:

- $\theta(0) = \pi/2$ the star initially lies on the equatorial plane of the reference system
- $\dot{\theta} = 0$ its initial velocity is initially parallel to the equatorial plane
- the initial condition for $\dot{t}$ descends from the normalization after requiring $g_{\mu\nu}u^\mu u^\nu = -c^2$
- Initial conditions for r and ϕ, on the other hand, can be inferred from the orbital elements.

$$(x_{\rm orb}, y_{\rm orb}) = (-a(1+e), 0),$$

$$(v_{\rm x,orb}, v_{\rm y,orb}) = \left(0, \frac{2\pi}{T}\frac{a^2}{r}\sqrt{1-e^2}\right)$$

semimajor axis

eccentricity

orbital period

Modelling the orbital motion of S2 star

The orbit of the S2 star in a generic metric is fully determined once the following parameters are set:

$$(M_\bullet, R_\bullet, T, t_p, a, e, i, \Omega, \omega, x_0, v_{x,0}, y_0, v_{y,0}, v_{\mathrm{LSR}}, \alpha)$$

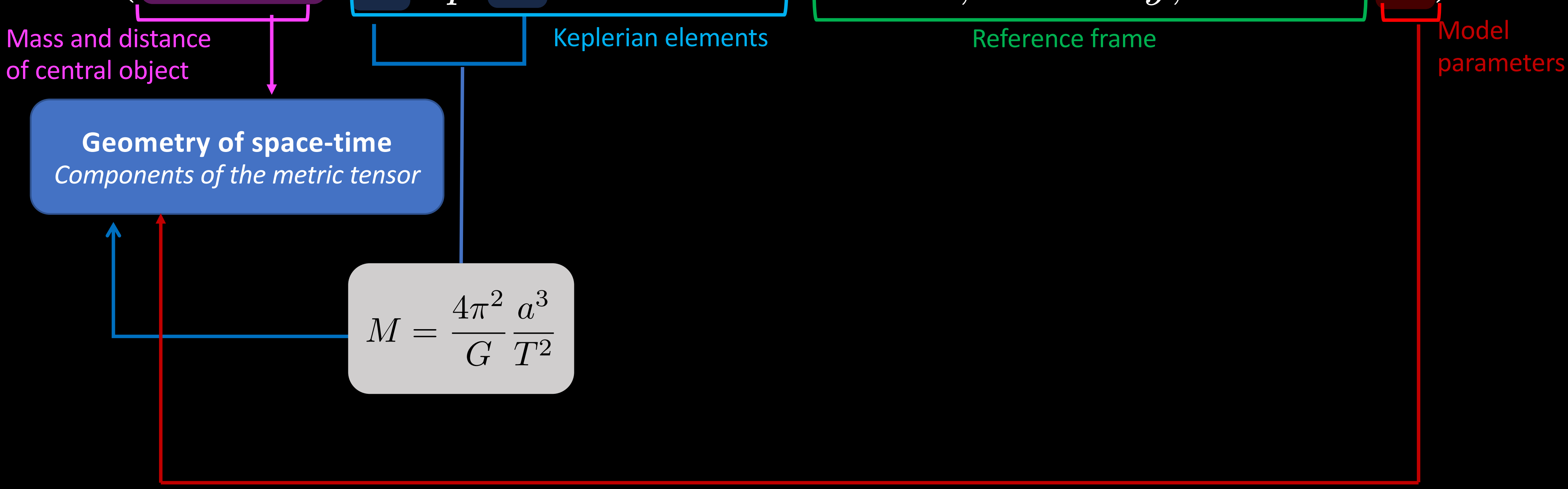

Modelling the orbital motion of S2 star

The orbit of the S2 star in the a genenric metric is fully determined once the following parameters are set:

$$(M_\bullet, R_\bullet, T, t_p, a, e, i, \Omega, \omega, x_0, v_{x,0}, y_0, v_{y,0}, v_{\mathrm{LSR}}, \alpha)$$

Mass and distance of central object

Keplerian elements

Reference frame

Model parameters

Geometry of space-time
Components of the metric tensor

Equations of motion
Geodesic eqs. related to metric

Initial data

Modelling the orbital motion of S2 star

The orbit of the S2 star in the a genenric metric is fully determined once the following parameters are set:

$$(M_\bullet, R_\bullet, T, t_p, a, e, i, \Omega, \omega, x_0, v_{x,0}, y_0, v_{y,0}, v_{\mathrm{LSR}}, \alpha)$$

Mass and distance of central object

Keplerian elements

Reference frame

Model parameters

Geometry of space-time
Components of the metric tensor

Equations of motion
Geodesic eqs. related to metric

Initial data

Star's trajectory
In the BH reference frame

Geometric projection & relativistic redshift

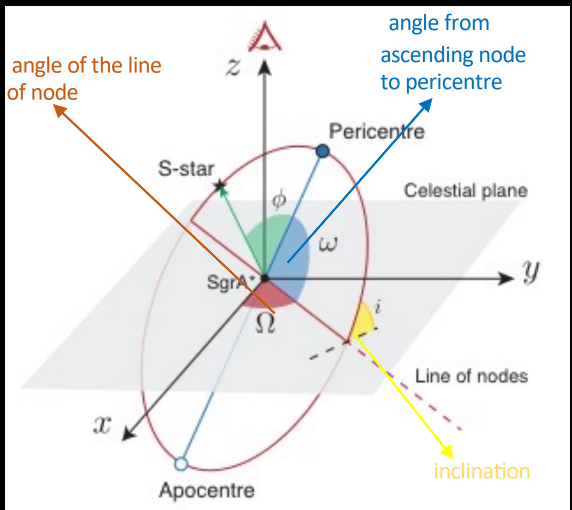

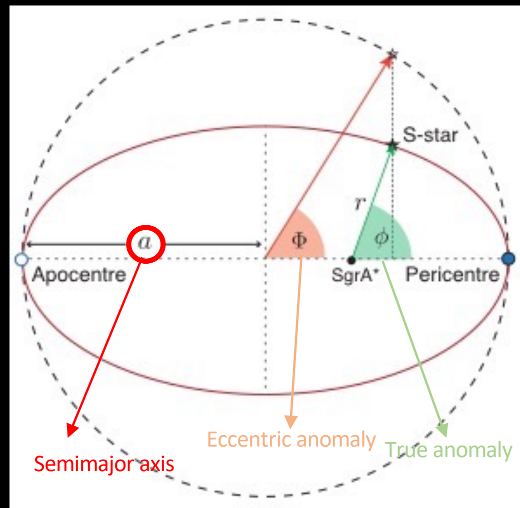

Modelling the orbital motion of S2 star

The orbit of the S2 star in the a genenric metric is fully determined once the following parameters are set:

$$(M_\bullet, R_\bullet, T, t_p, a, e, i, \Omega, \omega, x_0, v_{x,0}, y_0, v_{y,0}, v_{\mathrm{LSR}}, \alpha)$$

Mass and distance of central object — Keplerian elements — Reference frame — Model parameters

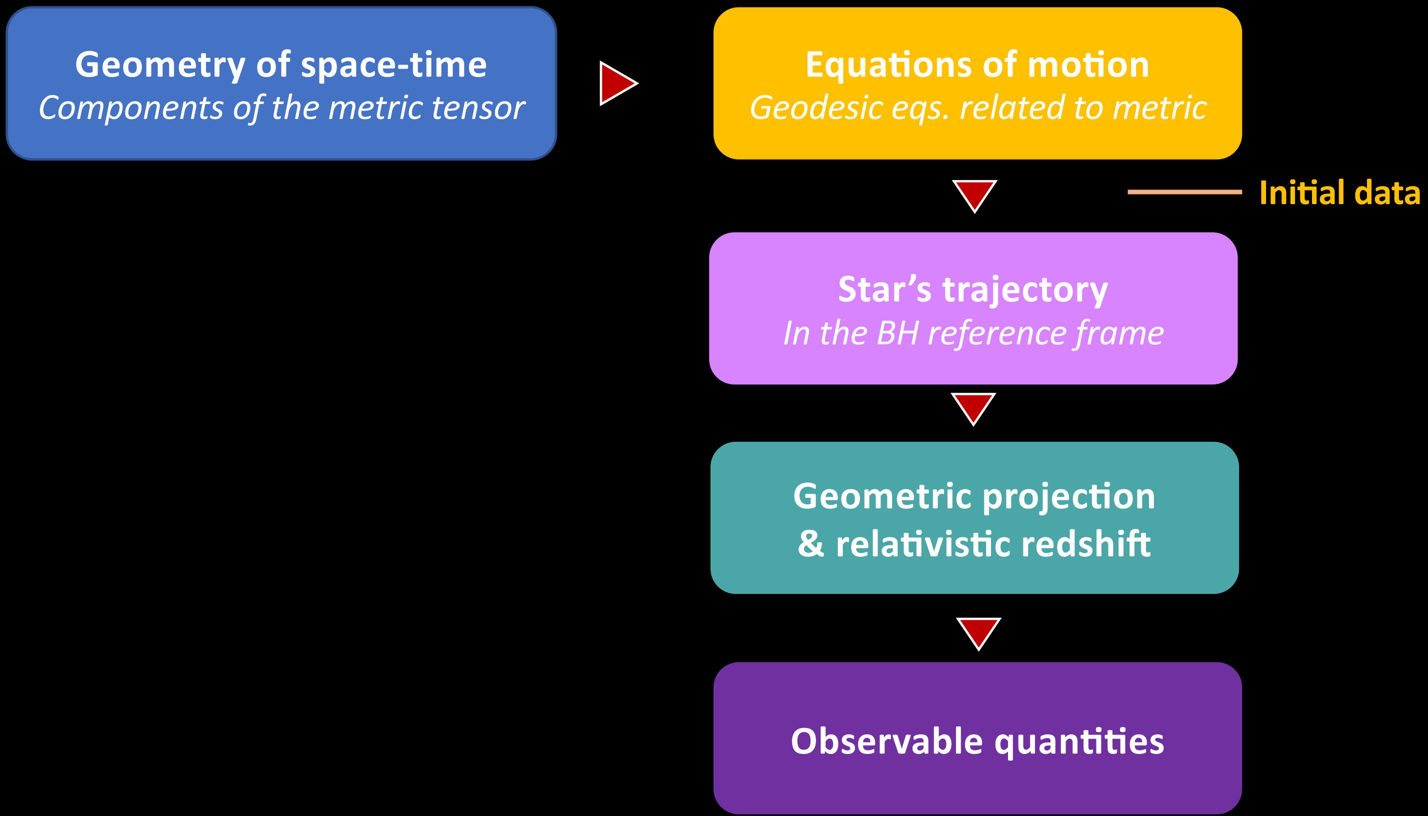

Modelling the orbital motion of S2 star

The orbit of the S2 star in the a genenric metric is fully determined once the following parameters are set:

$$(M_\bullet, R_\bullet, T, t_p, a, e, i, \Omega, \omega, x_0, v_{x,0}, y_0, v_{y,0}, v_{\rm LSR}, \alpha)$$

Mass and distance of central object ($M_\bullet, R_\bullet$)

Keplerian elements ($T, t_p, a, e, i, \Omega, \omega$)

Reference frame ($x_0, v_{x,0}, y_0, v_{y,0}, v_{\rm LSR}$)

Model parameters (α)

Geometry of space-time
Components of the metric tensor

▶

Equations of motion
Geodesic eqs. related to metric

— **Initial data**

▼

Star's trajectory
In the BH reference frame

▼

Geometric projection & relativistic redshift

▼

Observable quantities

▶

Fully relativistic mock orbit

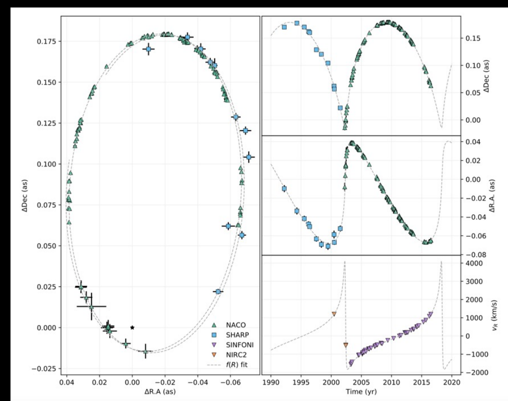

At least 13 parameters + that describe the model

Markov Chain Monte Carlo (MCMC) algorithm implemented in ***emcee.***

Data of the orbital motion of S2 star

- ✓ 145 data points representing the position of S2 in the K or H bands, relative to the 'Galactic Centre infrared reference system', from 1992.225 to 2016.38. The radio calibrations used to measure relative positions between stars in the nuclear cluster, by which the SHARP and NACO positions of S2 in the GC reference systems have been retrieved, can still be affected by a zero-point offset and a drift of the radio-reference frame with respect to the infrared reference frame. This translates into four additional reference frame parameters in the fitting procedure, $(x_0, y_0, v_{x,0}, v_{y,0})$, to account for this effect. For this purpose, we use the radio-to-infrared reference frame results as a prior:

$$\boldsymbol{x_0} = \boldsymbol{-0.2 \pm 0.2} \text{ mas} \qquad \boldsymbol{y_0} = \boldsymbol{0.1 \pm 0.2} \text{ mas}$$
$$\boldsymbol{v_{x,0}} = \boldsymbol{0.02 \pm 0.1} \text{ mas/yr} \qquad \boldsymbol{v_{y,0}} = \boldsymbol{0.06 \pm 0.1} \text{ mas/yr.}$$

- ✓ 44 data points for the radial velocity of S2 that have been collected at the Keck observatory before 2003, and at the VLT after 2003.
- ✓ 1 measurement of the departure from the Schwarzschild precession: f_{SP} = 1.10 ± 0.19

Gillessen, S., et al. 2017, ApJ, 837, 30
Gillessen, S., et al. 2009, ApJ Lett, 707, L114
Gravity Collaboration 2020, A&A, 636, L5

Unfortunately, GRAVITY data are not publicly available

f(R)-theory

An example: The simplest extension

The simplest extension of GR is given by the action

$$\mathcal{A} = \int d^4x\sqrt{-g}f(R)$$

$$f'(R)R_{\mu\nu} - \frac{f(R)}{2}g_{\mu\nu} = \nabla\mu\nabla_\nu f'(R) - g_{\mu\nu}\Box f'(R)$$

$$3\Box f'(R) + f'(R)R - 2f(R) = 0$$

$$f(R) = \sum_n \frac{f^n(R_0)}{n!}(R-R_0)^n$$

$$\simeq f_0 + f_0'R + f_0''R^2 + f_0'''R^3 + \ldots$$

One can derive a weak field spherically symmetric solution by solving the fourth-order field equations in the post-Newtonian limit of a spherically symmetric metric by matching at infinity the Minkowski space-time

$$ds^2 = [1+\Phi(r)]\,dt^2 - [1-\Phi(r)]\,dr^2 - r^2 d\Omega.$$

strength and the scale length

$$\Phi(r) = -\frac{2GM}{(1+\delta)rc^2}\left(1+\delta e^{-\frac{r}{\lambda}}\right)$$

A. De Felice, S. Tsujikawa Living Review, 13, 3 (2010)
S. Capozziello, M. De Laurentis, Annalen der Physik 524, 545 (2012)
S. Nojiri, S.D. Odintsov, Phys. Rep. 505, 59 (2011)
S. Capozziello, M. De Laurentis Phys.Rept. 509, 167 (2011)
T.P. Sotiriou and V. Faraoni, Rev. Mod. Phys. 82, 451 (2010)

f(R)-theory

S2 star data

16 parameters that entirely describe the model : 6 orbital parameters, 2 source parameters, 5 system reference parameters 2 extra parameters

	Uniform priors	
Parameter	Start	End
$M_\bullet$ ($10^6 M_\odot$)	3	5
$R_\bullet$ (kpc)	6.5	9.5
a (mas)	0.115	0.136
e	0.85	0.9
i ($^\circ$)	130	138
Ω ($^\circ$)	223	231
ω ($^\circ$)	60	70
$v_{\rm LSR}$ (km/s)	-50	50
δ	-0.9	2
λ (AU)	100	50 000

To not bias the result

	Gaussian priors	
	σ	μ
T (yr)	16.0455	0.013
$t_p - 2018$ (yr)	2018.37900	0.0016
x_0 (mas)	-0.2	0.01
y_0 (mas)	0.1	0.2
$v_{x,0}$ (mas/yr)	0.05	0.1
$v_{y,0}$ (mas/yr)	0.06	0.1

R. Della Monica, I. de Martino, M. De Laurentis Phys.Rev.D 104, 10 (2021)
M. De Laurentis, I. De Martino, and R. Lazkoz, PRD 97, 104068 (2018)
De Martino, R. Lazkoz, and M. De Laurentis PRD D 97, 104067 (2018).
M. De Laurentis, I. De Martino, and R. Lazkoz, EPJ C78, 916 (2018).

f(R)-theory

Results from f(R)-gravity

w/o orbital precession

68%, 95% and 99% confidence levels of the posterior probability density distributions for the entire set of parameters

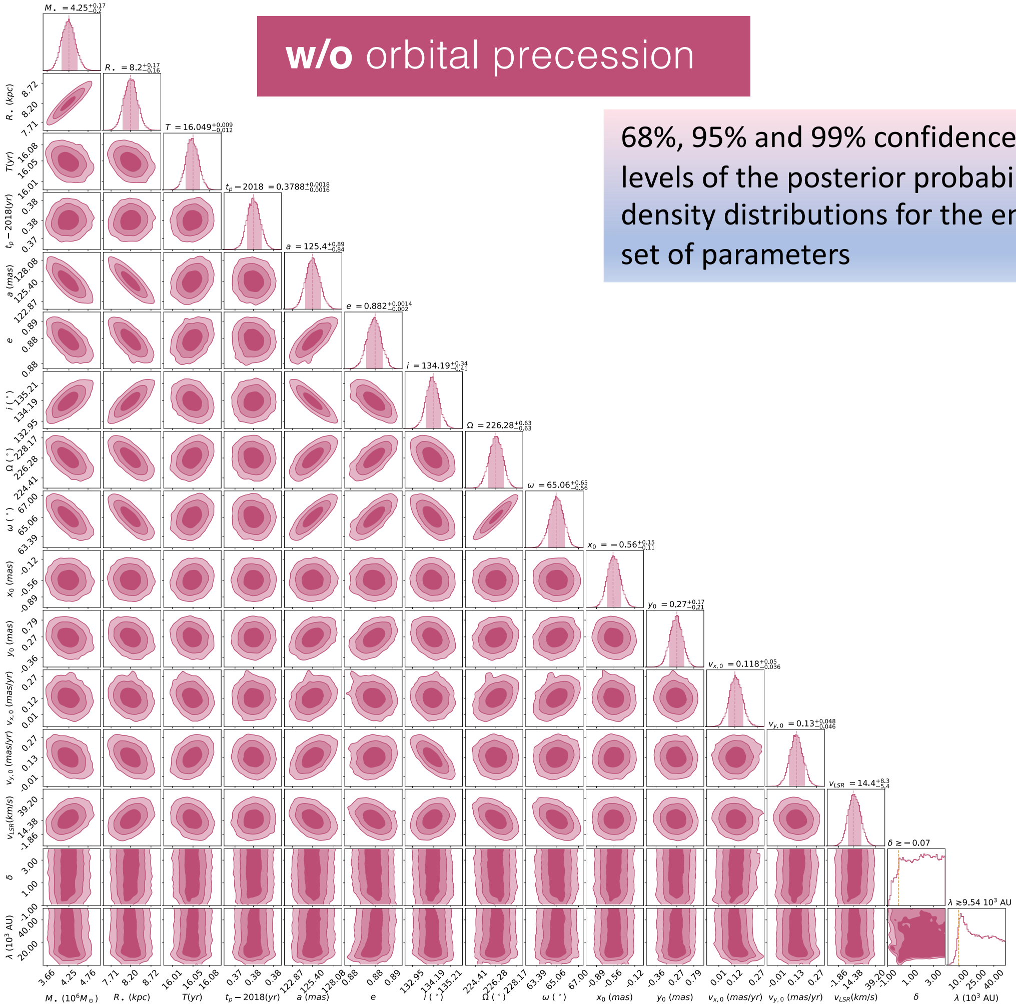

w/ orbital precesison

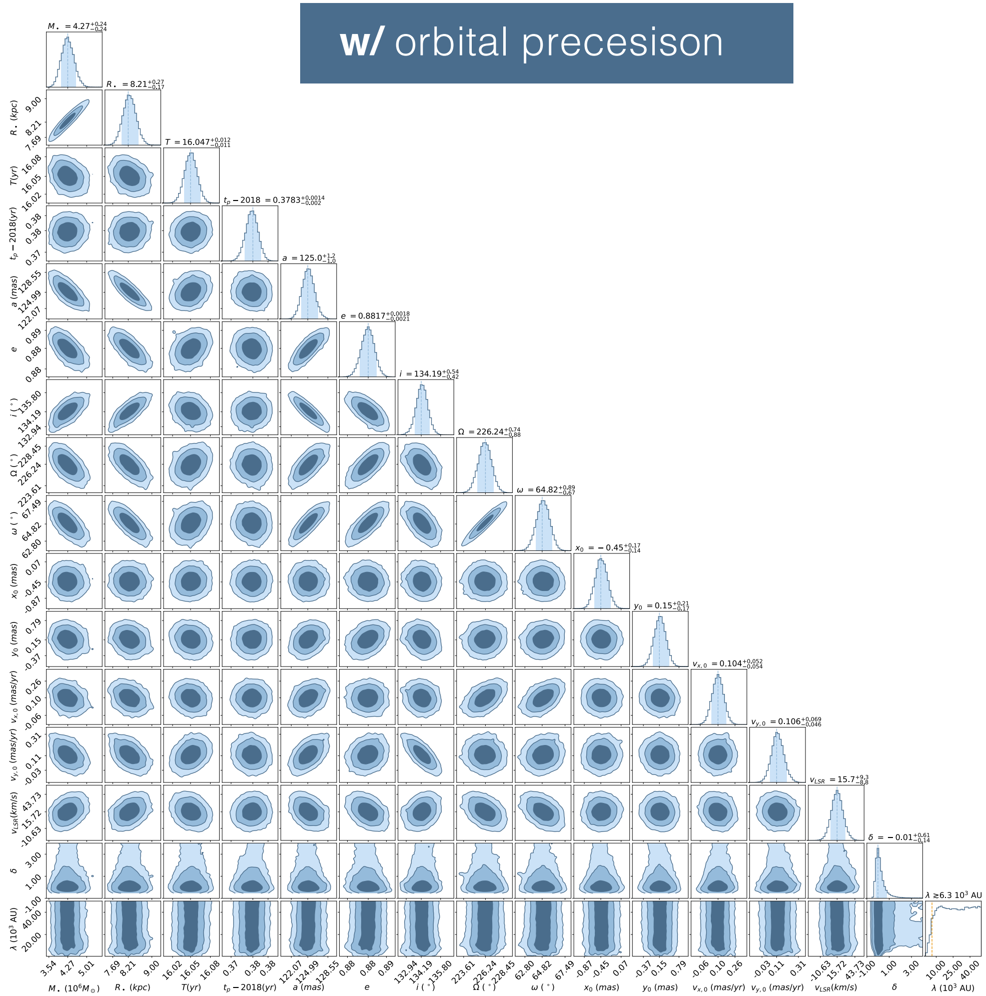

Results from f(R)-gravity

f(R)-theory

w/o orbital precession

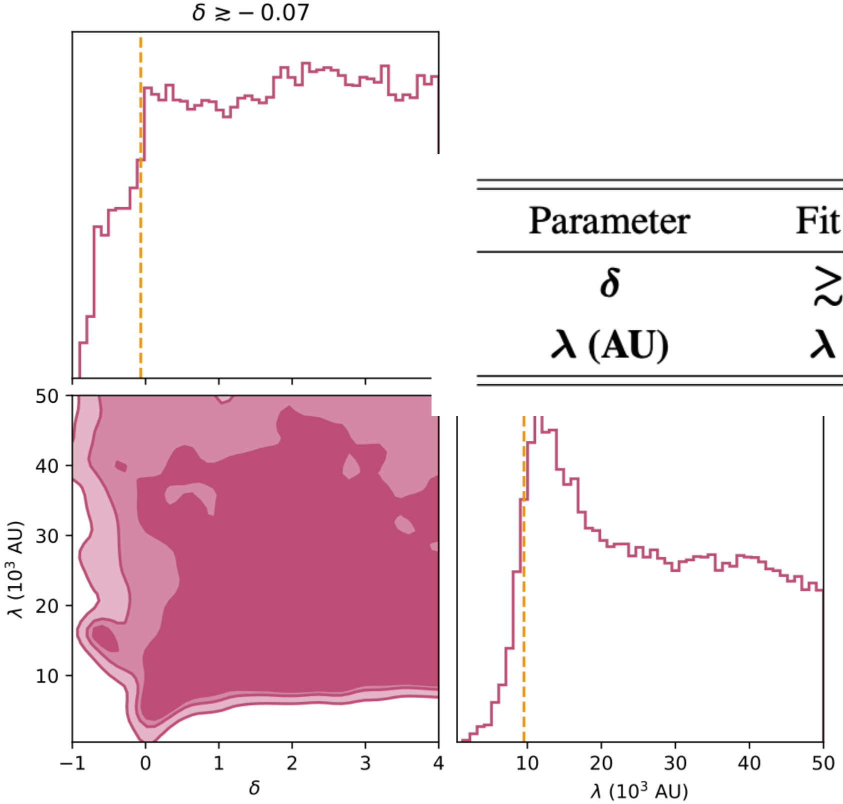

w/ orbital precesison

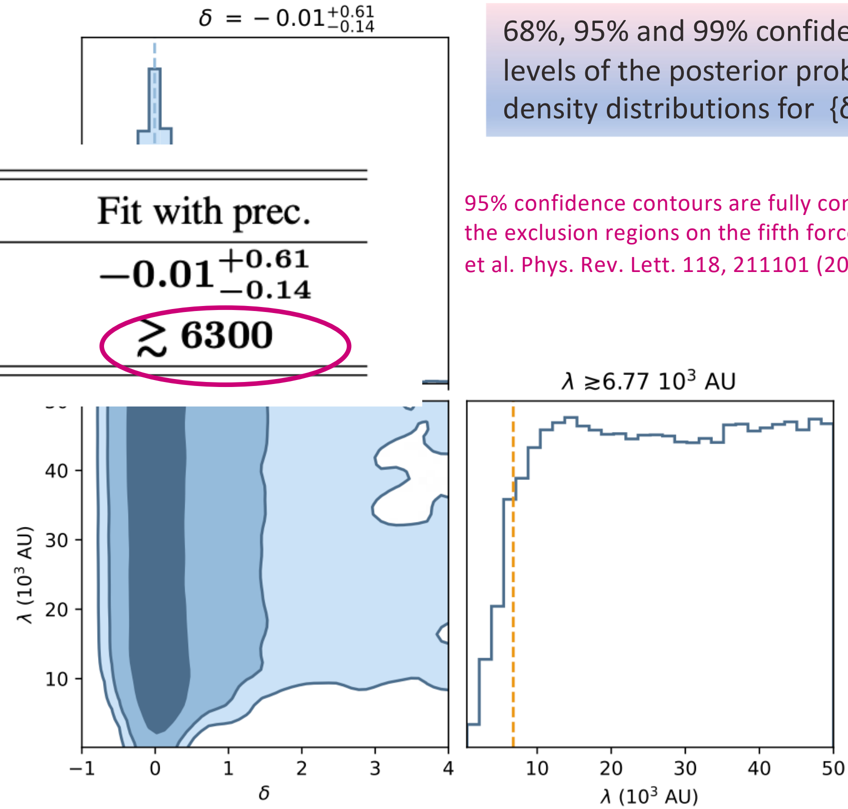

Parameter	Fit w/o prec.	Fit with prec.
$\boldsymbol{\delta}$	$\gtrsim -0,07$	$-0.01^{+0.61}_{-0.14}$
$\boldsymbol{\lambda}$ (AU)	$\lambda \gtrsim 9540$	$\gtrsim 6300$

68%, 95% and 99% confidence levels of the posterior probability density distributions for {δ, λ}

95% confidence contours are fully consistent with the exclusion regions on the fifth force Hees, Ghez et al. Phys. Rev. Lett. 118, 211101 (2017)

Horndeski Theory

Weak field limit in Horndeski Theory

The gravitational action of Horndeski theory takes the following form:

denotes all matter fields

$$S = \sum_{i=2}^{5} \int d^4x \sqrt{-g}\, \mathcal{L}_i[g_{\mu\nu}, \phi] + S_m[g_{\mu\nu}, \chi_m]$$

matter action

The gravitational part of the action, which depends on the metric $g_{\mu\nu}$ and one scalar field ϕ, is given by the following terms:

free functions of the scalar field ϕ and its kinetic term X

$$\mathcal{L}_2 = G_2(\phi, X)\,, \quad \mathcal{L}_3 = -G_3(\phi, X)\Box\phi\,,$$

$$\mathcal{L}_4 = G_4(\phi, X)R + G_{4X}(\phi, X)\left[(\Box\phi)^2 - (\nabla_\mu\nabla_\nu\phi)^2\right]\,,$$

$$\mathcal{L}_5 = G_5(\phi, X)G_{\mu\nu}\nabla^\mu\nabla^\nu\phi - \frac{1}{6}G_{5X}(\phi, X)\left[(\Box\phi)^3 - 3(\Box\phi)(\nabla_\mu\nabla_\nu\phi)^2 + 2(\nabla_\mu\nabla_\nu\phi)^3\right]$$

Hohmann M., 2015, Phys. Rev. D, 92, 064019
G. W. Horndeski, Int. JTP 10, 363 (1974)
T. Kobayashi, M. Yamaguchi, and J. Yokoyama, PTP. 126, 511 (2011)

Horndeski Theory

Weak field limit in Horndeski Theory

For a mass point source the solution at Newtonian order is

$$h_{00}^{(2)}(r) = \frac{M}{4\pi r}\left[c_2 + \frac{c_1 c_\psi}{m_\psi^2}\left(e^{-m_\psi r} - 1\right)\right]$$

$$c_1 = -2\frac{G_{4(1,0)}G_{2(2,0)}}{G_{4(0,0)}\Upsilon}\,, \quad c_2 = \frac{1}{2G_{4(0,0)}} + \frac{G_{4(1,0)}^2}{2G_{4(0,0)}^2\Upsilon} \quad m_\psi = \sqrt{\frac{-2G_{2(2,0)}}{\Upsilon}}\,, \quad c_\psi = \frac{G_{4(1,0)}}{2G_{4(0,0)}}\Upsilon^{-1}$$

Where for sake of simplicity we have introduced the following definition

$$\Upsilon \equiv K_{(0,1)} - 2G_{3(1,0)} + 3\frac{G_{4(1,0)}^2}{G_{4(0,0)}}$$

Horndeski Theory

Weak field limit in Horndeski Theory

For a mass point source the solution at Newtonian order is

$$h_{00}^{(2)}(r) = \frac{M}{4\pi r}\left[c_2 + \frac{c_1 c_\psi}{m_\psi^2}(e^{-m_\psi r} - 1)\right]$$

$$c_1 = -2\frac{G_{4(1,0)}G_{2(2,0)}}{G_{4(0,0)}\Upsilon}, \quad c_2 = \frac{1}{2G_{4(0,0)}} + \frac{G_{4(1,0)}^2}{2G_{4(0,0)}^2\Upsilon} \quad m_\psi = \sqrt{\frac{-2G_{2(2,0)}}{\Upsilon}}, \quad c_\psi = \frac{G_{4(1,0)}}{2G_{4(0,0)}}\Upsilon^{-1}$$

Where for sake of simplicity we have introduced the following definition

$$\Upsilon \equiv K_{(0,1)} - 2G_{3(1,0)} + 3\frac{G_{4(1,0)}^2}{G_{4(0,0)}}$$

$\Upsilon > 0$ Implies $G_{2(0,0)} < 0$ = reducing allowed parameter space

The metric perturbation becomes:

$$h_{00}^{(2)}(r) = \frac{M}{4\pi r}\left[\frac{1}{2G_{4(0,0)}} + \frac{1}{2}\left(\frac{G_{4(1,0)}}{G_{4(0,0)}}\right)^2\Upsilon^{-1}e^{-m_\psi r}\right]$$

plays the role of the inverse of gravitation constant *G*

G. W. Horndeski, Int. JTP 10, 363 (1974)
T. Kobayashi, M. Yamaguchi, and J. Yokoyama, PTP. 126, 511 (2011)
M. Hohmann, Phys. Rev. D 92, 064019 (2015)

Geodesic Motion in Horndeski theory

Our baseline model has 18 parameters: 6 orbital parameters, 2 source parameters, 5 system reference parameters, 5 extra parameters

Parameter	Unit	Value	Error	Parameter	Unit	Value	Error
$M_\bullet$	$10^6 M_\odot$	4.35	0.012	$y_\bullet$	mas	0.1	0.2
$R_\bullet$	kpc	8.33	0.0093	$v_{x,\bullet}$	mas/yr	0.02	0.2
a	mas	125.5	0.044	$v_{y,\bullet}$	mas/yr	0.06	0.1
e		0.8839	0.000079	$v_{z,\bullet}$	km/s	0	5
i	$\circ$	134.18	0.033			**Interval**	
ω	$\circ$	65.51	0.030	$G_{4(0,0)}$	$M_\odot \mathrm{AU/s^2}$	$[0.95, 1.05](c^4/16\pi G)$	
Ω	$\circ$	226.94	0.031	$G_{4(1,0)}$	$M_\odot \mathrm{AU/s^2}$	[-100, 100]	
T	yr	16.00	0.0013	$G_{3(1,0)}$	$M_\odot \mathrm{AU/s^2}$	[-100000, 100000]	
t_p	yr	2018.33	0.00017	$G_{2(0,1)}$	$M_\odot \mathrm{AU/s^2}$	[-100000, 100000]	
$x_\bullet$	mas	−0.2	0.2	$G_{2(2,0)}$	$M_\odot \mathrm{/AUs^2}$	[-10, 0]	

R Della Monica, I de Martino, D Vernieri, M De Laurentis, MNRAS 159, 1981 (2023)

Horndeski Theory

Geodesic Motion in Horndeski theory

Modulate the strength and scale length of the modification to the Newtonian potential

$G_{4(0,0)} = c^4/16\pi G_N$

varying values for the Horndeski-Taylor coefficients

give a value of $1/m_\psi$ that is a given fraction of the typical scale length of the S2 orbit

toy models for S2 with the same orbital parameters

Model	$1/m_\psi$	$G_{4(0,0)}$	$G_{4(1,0)}$	$G_{3(1,0)}$	$G_{2(0,1)}$	$G_{2(2,0)}$
	(AU)	$(M_\odot \mathrm{AU/s^2})$	$(M_\odot \mathrm{AU/s^2})$	$(M_\odot \mathrm{AU/s^2})$	$(M_\odot \mathrm{AU/s^2})$	$(M_\odot \mathrm{/AUs^2})$
(1)	(2)	(3)	(4)	(5)	(6)	(7)
Toy 1	0.0	8.0940	0	0	0	0
Toy 2	66.0	8.0940	10	0	50	-0.01
Toy 3	208.6	8.0940	10	0	50	-0.001
Toy 4	433.4	8.0940	100	0	50	-0.01
Toy 5	1370.5	8.0940	100	0	50	-0.001

star moving under the influence of an unperturbed Newtonian potential

R Della Monica, I de Martino, D Vernieri, M De Laurentis, MNRAS 159, 1981 (2023)

Horndeski Theory

Geodesic Motion in Horndeski theory

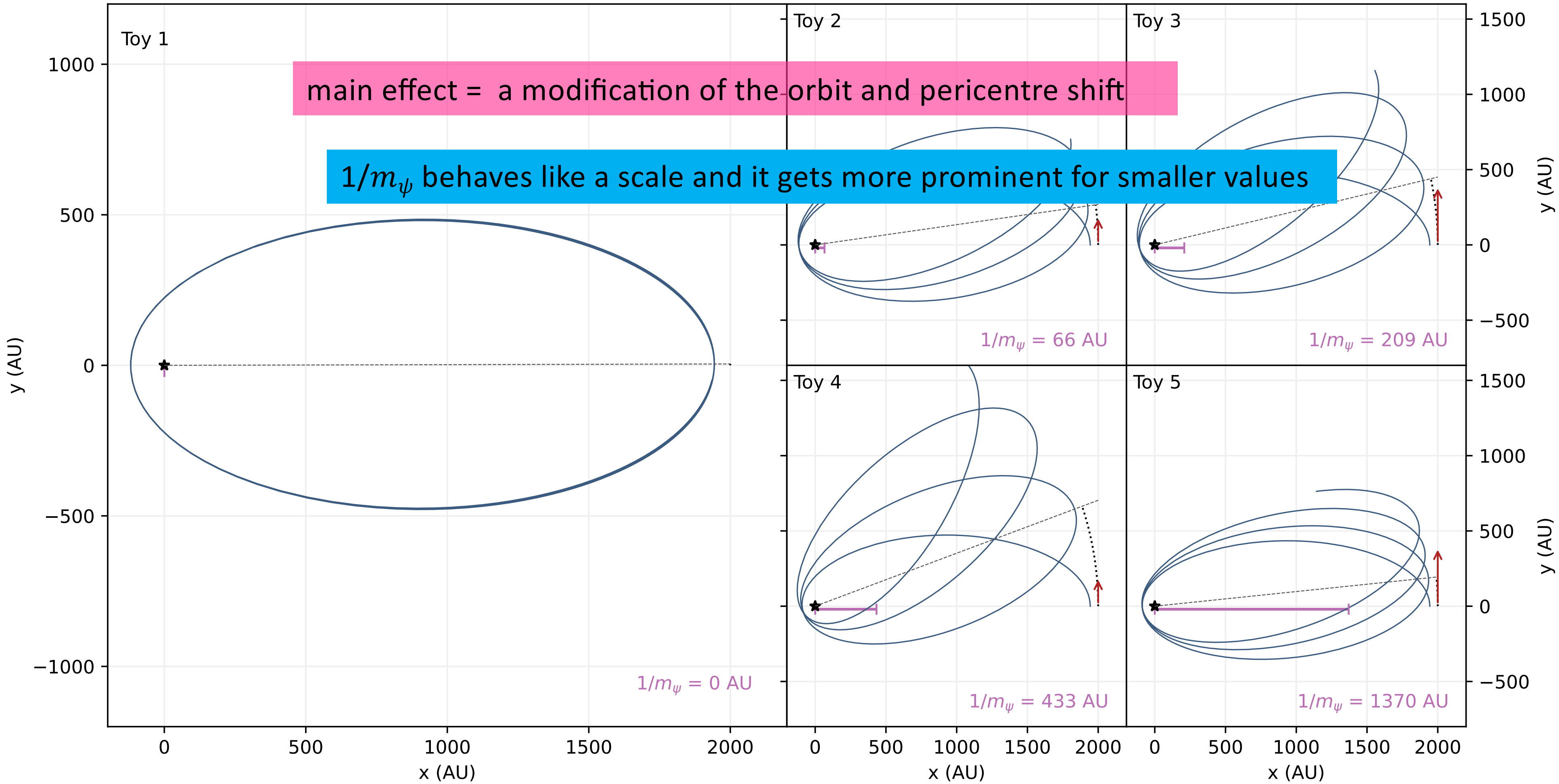

main effect = a modification of the orbit and pericentre shift

$1/m_\psi$ behaves like a scale and it gets more prominent for smaller values

R Della Monica, I de Martino, D Vernieri, M De Laurentis, MNRAS 159, 1981 (2023)

Observational constraints from S2-star: Results

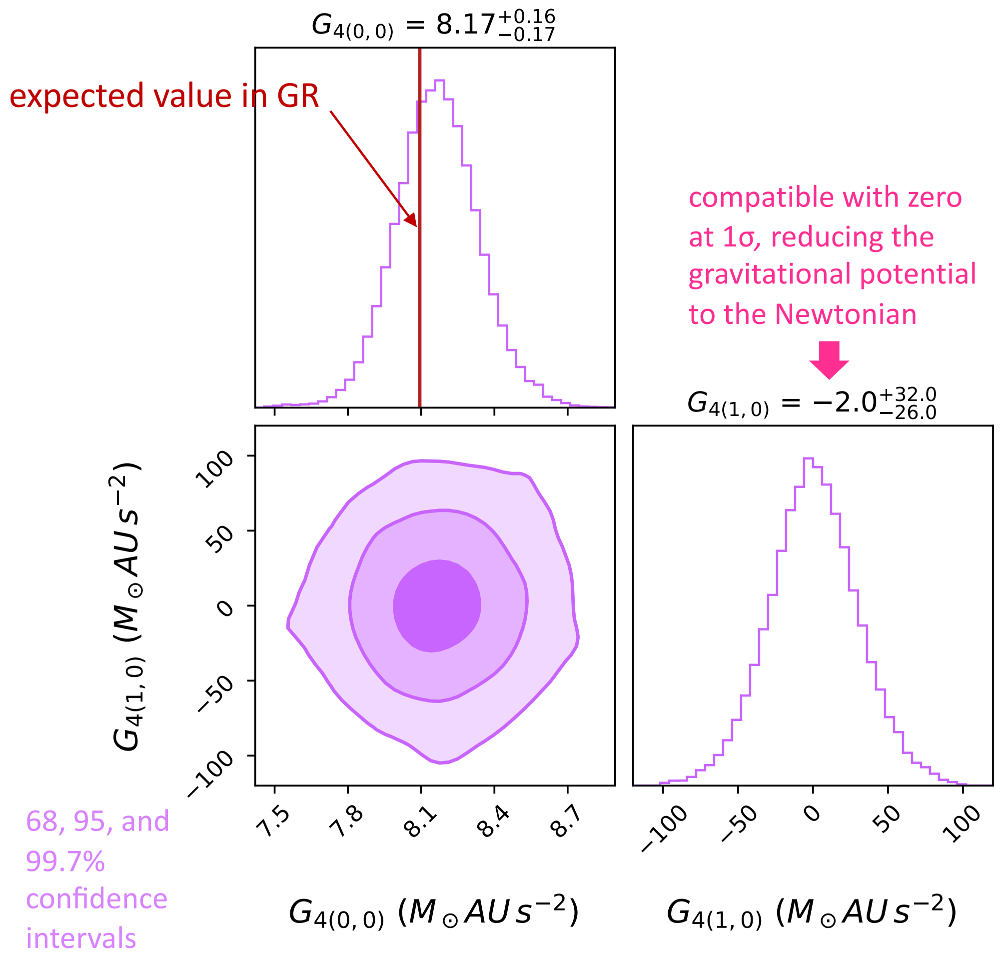

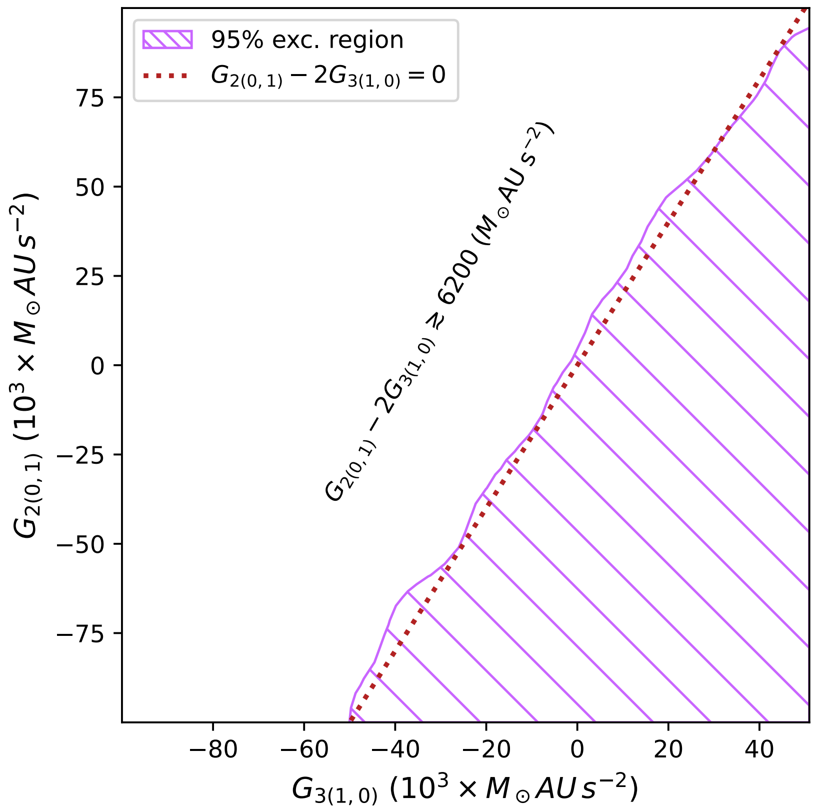

Horndeski Theory

Observational constraints from S2-star: Results

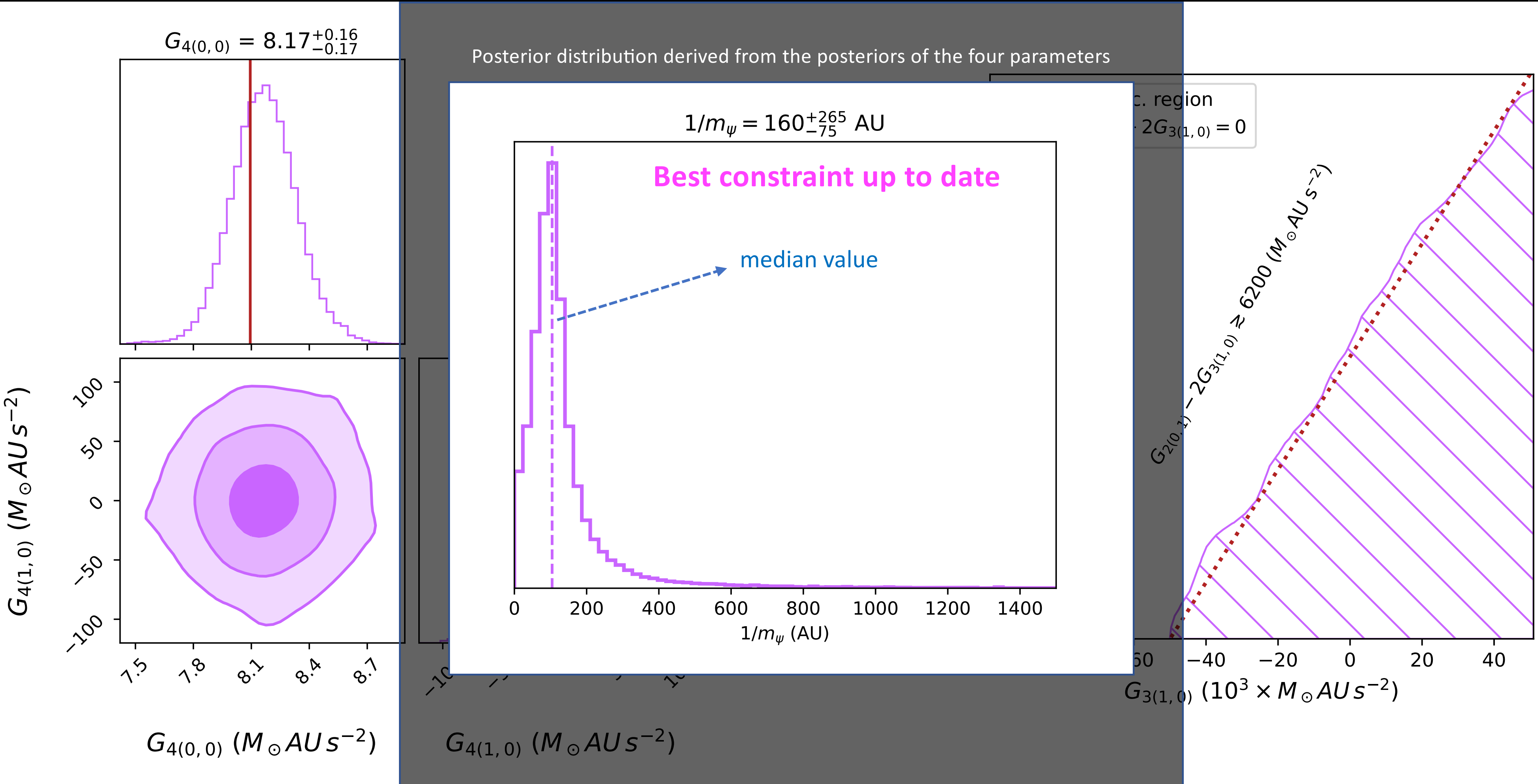

R Della Monica, I de Martino, D Vernieri, M De Laurentis, MNRAS 159, 1981 (2023)

First take away points

Using the orbital motion of the S2 star around SgrA*, we have placed constraints on

Horndeski Theory

- On 2 Taylor coefficients of Horndeski theory and on a combination of the other 2 coefficients
- Our constraint shows full accordance with the GR value of $G4(1,0)$ = 0 within 1σ.
- A strong bound on the previously unbounded parameter $1/m_{\psi}$ was set

f(R)-theory

- Our analysis, thus, provides the first constraint on the strength of the Yukawa-like potential at the Galactic Centre: δ = −0.01+0.61
- we only obtain a lower bound on the scale length of the Yukawa-like potential: λ >6300 AU at 1σ.
- We do not detect any deviation from GR
- we converted our results in the constraints on first and second derivatives of the f(R) Lagrangian

STVG-theory

- In STVG in both approaches, we did not find any deviation from GR.
- α has not a lower bound, and it agrees with GR at 1σ
- α, has a mean value of 0.041 and an upper limit at 99,7% confidence level of ⍰ 0.548
- Up-to-date, this is the first constraint of STVG at scale of the SMBH on the center of our Galaxy

Second step: testing SgrA* space-time at horizon scale

Quantifying deviations from Kerr

We connect the predicted shadow size to an image diameter and compare it to the measured diameter

Shadow diameter

$$\hat{d}_m = \frac{\hat{d}_m}{d_{\rm sh}} d_{\rm sh} = \alpha_{\rm c}\, d_{\rm sh} = \alpha_{\rm c}\,(1+\delta)\, d_{\rm sh,Sch} = \alpha_{\rm c}\,(1+\delta)\, 6\sqrt{3}\,\theta_g$$

Measured ring diameter from imaging and model-fitting to the SgrA* data

Calibration factor determined by the physics of image formation near the horizon and quantifies the degree to which the image diameter tracks that of the shadow

$$\delta \equiv \frac{d_{\rm sh}}{d_{\rm sh,Sch}} - 1$$

Deviation parameter

Angular size corresponding to the M/D prior

$$\theta_g \equiv \frac{GM}{Dc^2}$$

$$d_{\rm sh,Sch} = 6\sqrt{3}\theta_g$$

$$\alpha_{\rm c} = \alpha_1 \times \alpha_2$$

α_1 is from the ray-traced image models

α_2 is from convolving these models with observational effects (scattering etc.) and reconstructing

We used this relation to infer the posterior on the deviation parameter given the EHT measurements and prior information

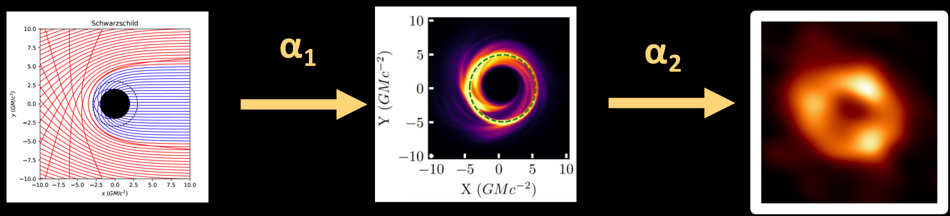

BH shadow — Emission ring in perfect image — Emission ring in reconstructed image

EHT paper VI-ApJ 930 (2022) 2, L17

Quantifying deviations from Kerr

We connect the predicted shadow size to an image diameter and compare it to the measured diameter

Shadow diameter

$$\hat{d}_m = \frac{\hat{d}_m}{d_{\rm sh}} d_{\rm sh} = \alpha_{\rm c}\, d_{\rm sh} = \alpha_{\rm c}\, (1+\delta)\, d_{\rm sh,Sch} = \alpha_{\rm c}\, (1+\delta)\, 6\sqrt{3}\, \theta_g$$

Measured ring diameter from imaging and model-fitting to the SgrA* data

Calibration factor determined by the physics of image formation near the

$$\delta \equiv \frac{d_{\rm sh}}{d_{\rm sh,Sch}} - 1$$

Deviation parameter

Angular size corresponding to the M/D prior

$$\theta_g \equiv \frac{GM}{Dc^2}$$

$$d_{\rm sh,Sch} = 6\sqrt{3}\theta_g$$

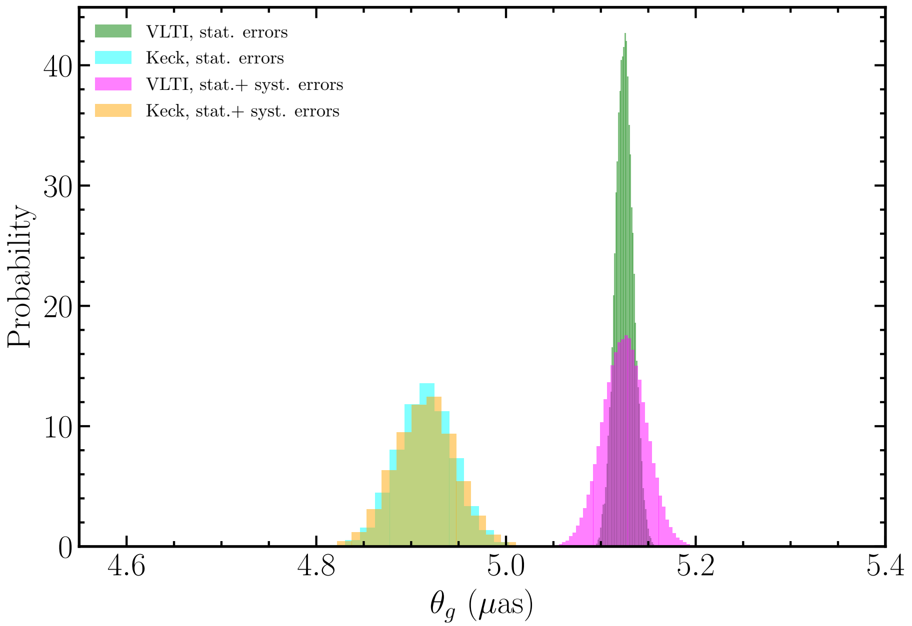

We used this relation to infer the posterior on the deviation parameter given the EHT measurements and prior information

Posteriors derived from the dynamical analyses of the orbit of S0-2 star by the Keck and the VLTI teams

EHT paper VI-ApJ 930 (2022) 2, L17

The α_1 Calibration Factor and its Uncertainties

We calibrate the relationship between the geometrically defined black hole shadow boundary and the observed size of the ring-like images using a large library that includes both Kerr and non-Kerr simulations.

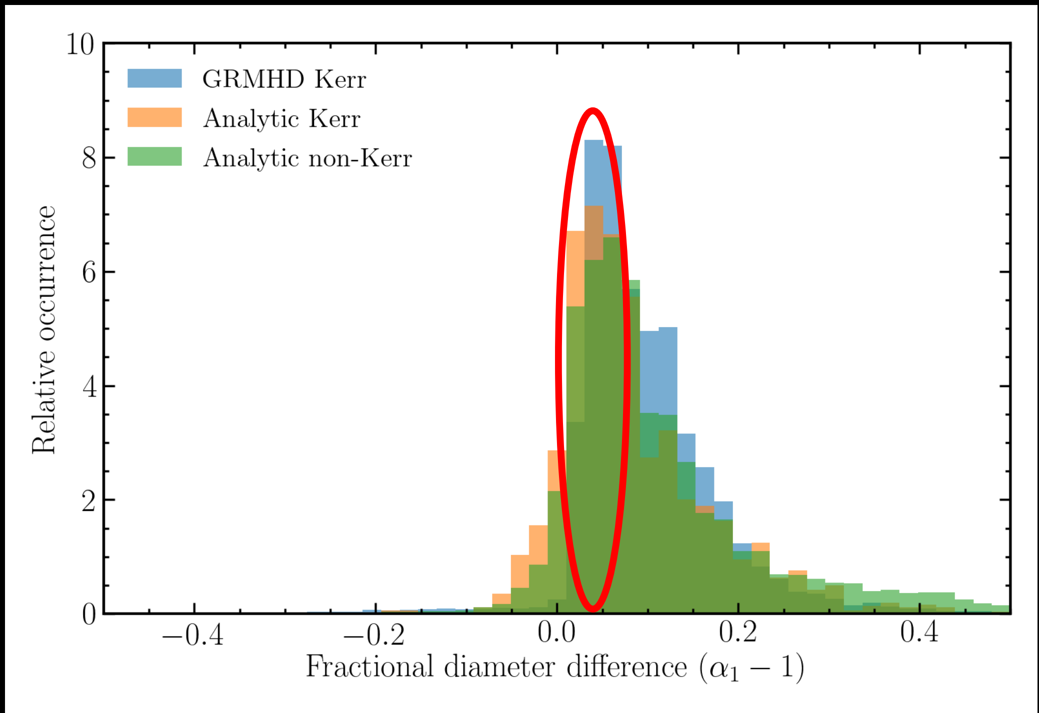

Fractional diameter difference between the diameter of peak emission in the image of a black hole and that of its shadow

Result from 180,000 snapshots from time-dependent GRMHD simulations in the Kerr metric

KHARMA (Prather et al. 2021)
BHAC (Porth et al. 2017)
ipole (Mościbrodzka & Gammie 2018)
BHOSS (Younsi et al.2012, 2016).

Analytic plasma models in the Kerr metric

Results for analytic plasma models in non-Kerr metric either parametrized metric

All distributions peak at small positive values indicate that the bright ring is slightly larger than the boundary of the black hole shadow.

The α_2 Calibration Factor and its Uncertainties

We then calibrate this relationship for reconstructed models

We conducted a blind analysis of about 150 synthetic data sets for both the imaging and model fitting pipelines.

Our synthetic data set included:

- images that matched the basic features of SgrA* data
- images that did not match the basic features of SgrA* data
- variable and non-variable data
- images of various ring sizes and morphologies both Kerr and non-Kerr images

The small offsets in the calibration parameter mimic those seen in the analysis of the actual Sgr A data.

Distribution peaks at small positive values.

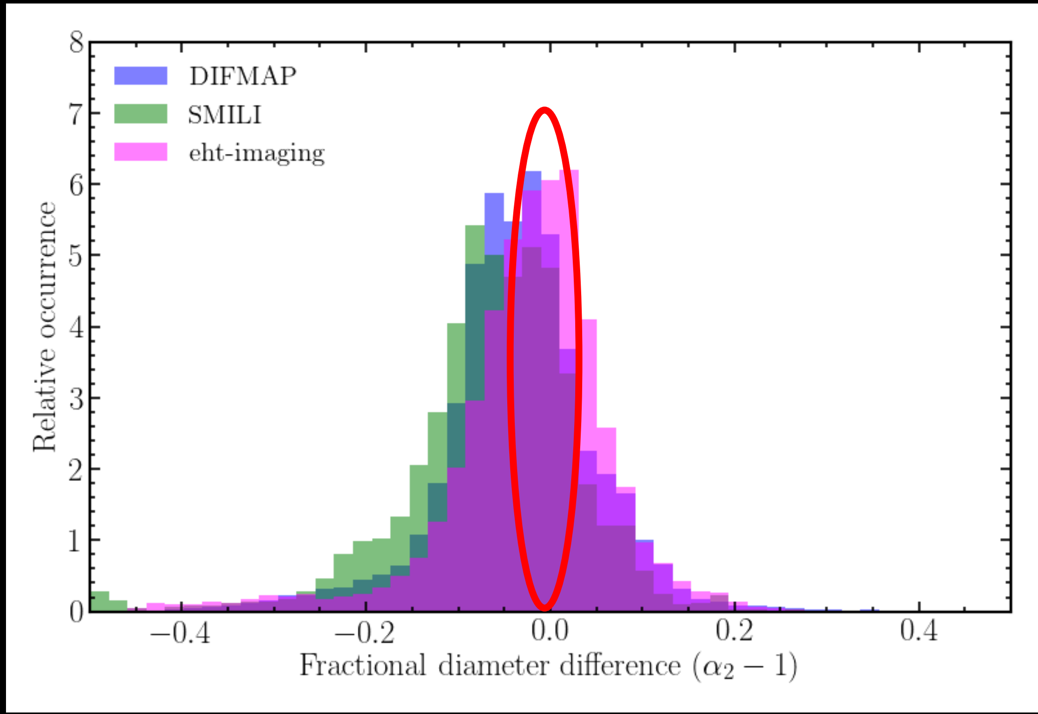

Fractional diameter difference between the diameter of peak emission in ground truth images and the those reconstructed

Özel et al. (2021) and Younsi et al. (2021)

Examples of images used for calibration

Simulated 1.3mm Sgr A* images for different spacetime geometries and plasma models

Field of view in all panels is 150 μas in both directions, with the brightest pixel value in each panel normalized to unity

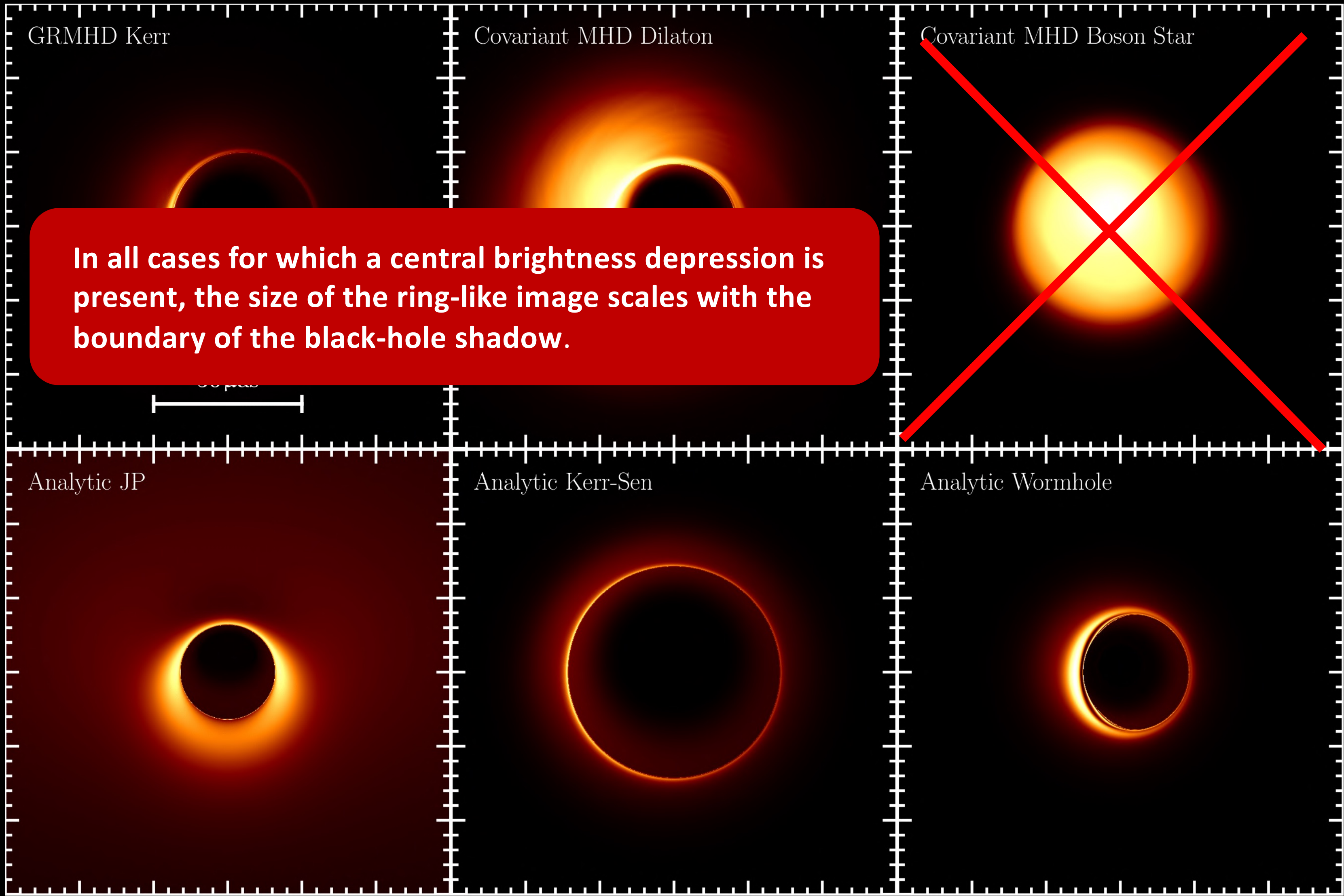

In all cases for which a central brightness depression is present, the size of the ring-like image scales with the boundary of the black-hole shadow.

The Diameter of the Black Hole Shadow

We used the exquisite prior constraints on the mass-to-distance ratio for Sgr A* based on stellar dynamics to show that the observed image size is within 10% of the Kerr predictions.

All of the posteriors are consistent with each other and with no deviation from GR predictions!!!

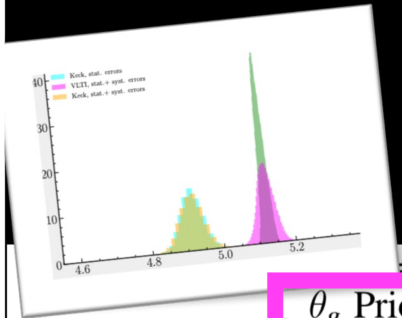

Deviation parameter

	θ_g Prior	GRMHD	Analytic Kerr	Analytic Non-Kerr
eht-imaging	VLT(I)	$-0.08^{+0.09}_{-0.09}$	$-0.05^{+0.09}_{-0.11}$	$-0.07^{+0.10}_{-0.09}$
	Keck	$-0.04^{+0.09}_{-0.10}$	$-0.02^{+0.11}_{-0.11}$	$-0.02^{+0.10}_{-0.09}$
SMILI	VLT(I)	$-0.10^{+0.12}_{-0.10}$	$-0.08^{+0.13}_{-0.11}$	$-0.08^{+0.12}_{-0.10}$
	Keck	$-0.06^{+0.13}_{-0.10}$	$-0.04^{+0.13}_{-0.11}$	$-0.04^{+0.13}_{-0.10}$
DIFMAP	VLT(I)	$-0.12^{+0.10}_{-0.08}$	$-0.10^{+0.09}_{-0.10}$	$-0.10^{+0.09}_{-0.09}$
	Keck	$-0.08^{+0.09}_{-0.09}$	$-0.07^{+0.10}_{-0.11}$	$-0.07^{+0.09}_{-0.09}$

means and 68th percentile credible levels for the posteriors

8% range predicted for the Kerr metric, depending on (a, i)

Posteriors on the parameter

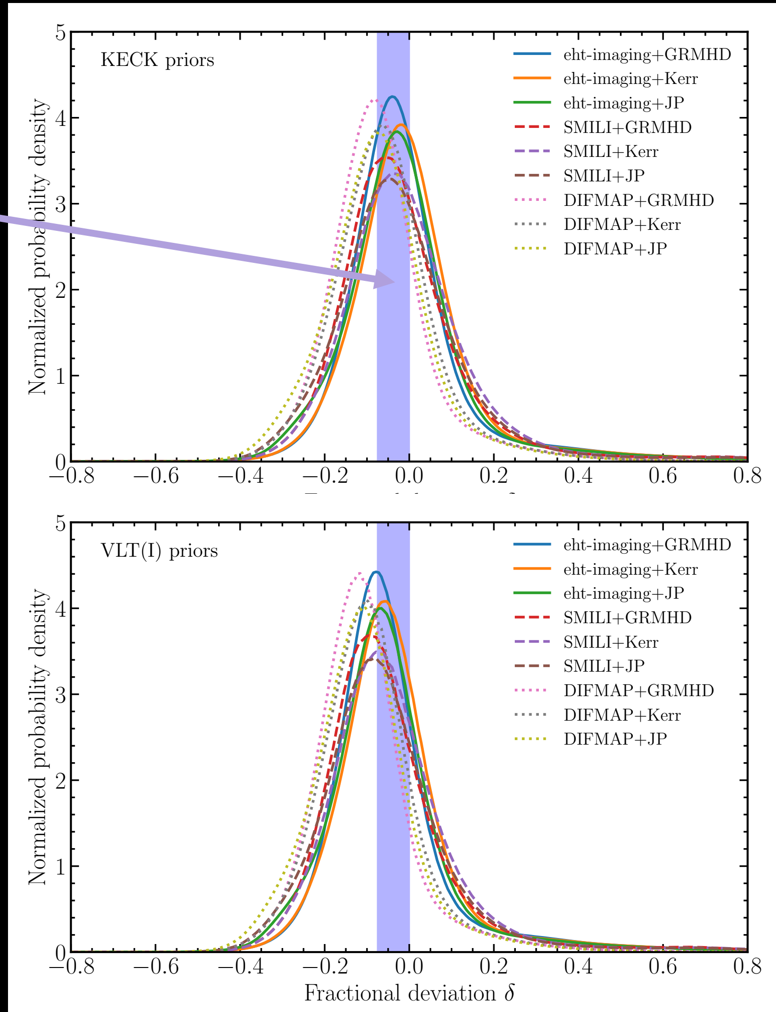

The Diameter of the Black-Hole Shadow

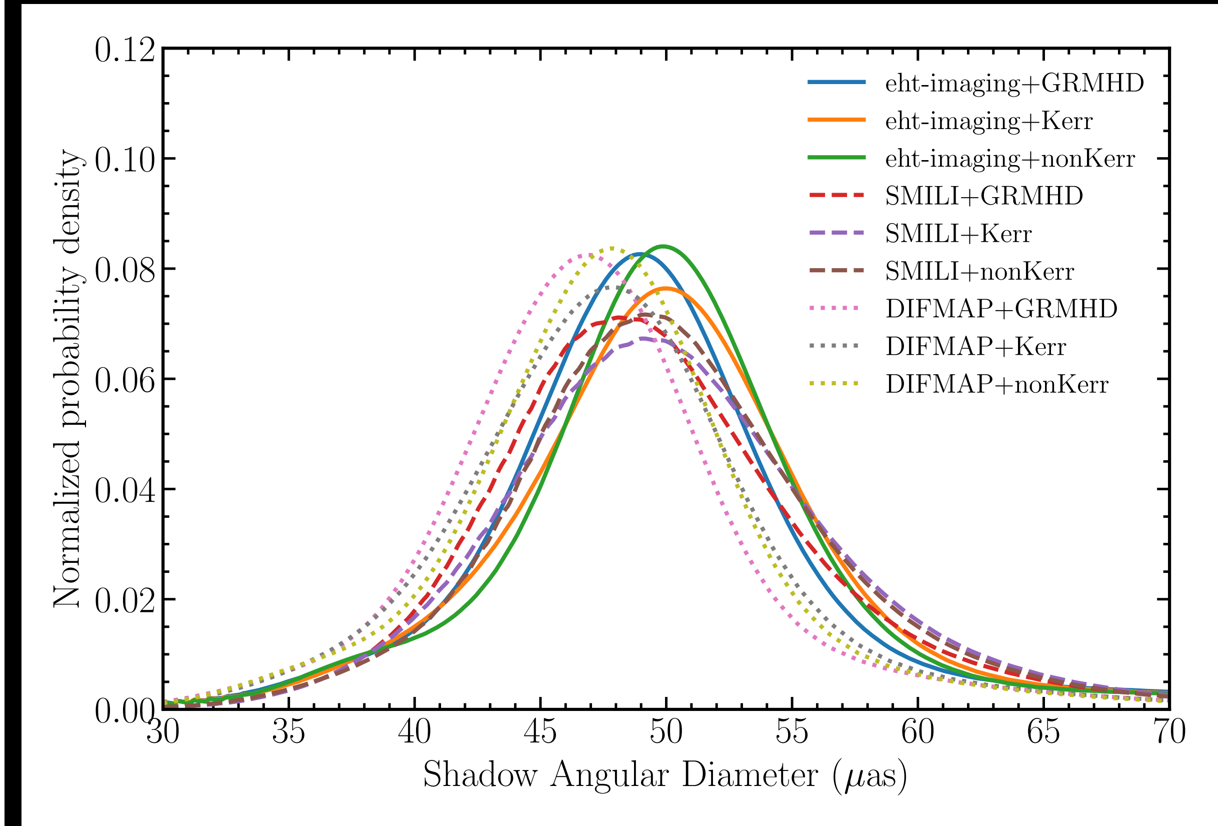

Posteriors over the shadow diameter inferred using the measurements of the ring diameter size based on three image-domain algorithms

We use the combination of the measurements and calibrations to infer the diameter of the boundary of the black hole shadow

	GRMHD	Analytic Kerr	Analytic non-Kerr
eht-imaging	$48.9^{+5.2}_{-5.1}$	$50.0^{+5.6}_{-5.6}$	$49.9^{+5.2}_{-4.9}$
SMILI	$48.1^{+6.3}_{-5.2}$	$49.1^{+6.5}_{-5.7}$	$49.2^{+6.2}_{-5.4}$
DIFMAP	$46.9^{+4.9}_{-5.2}$	$47.8^{+5.1}_{-5.7}$	$47.8^{+4.9}_{-5.2}$

The Diameter of the Black-Hole Shadow

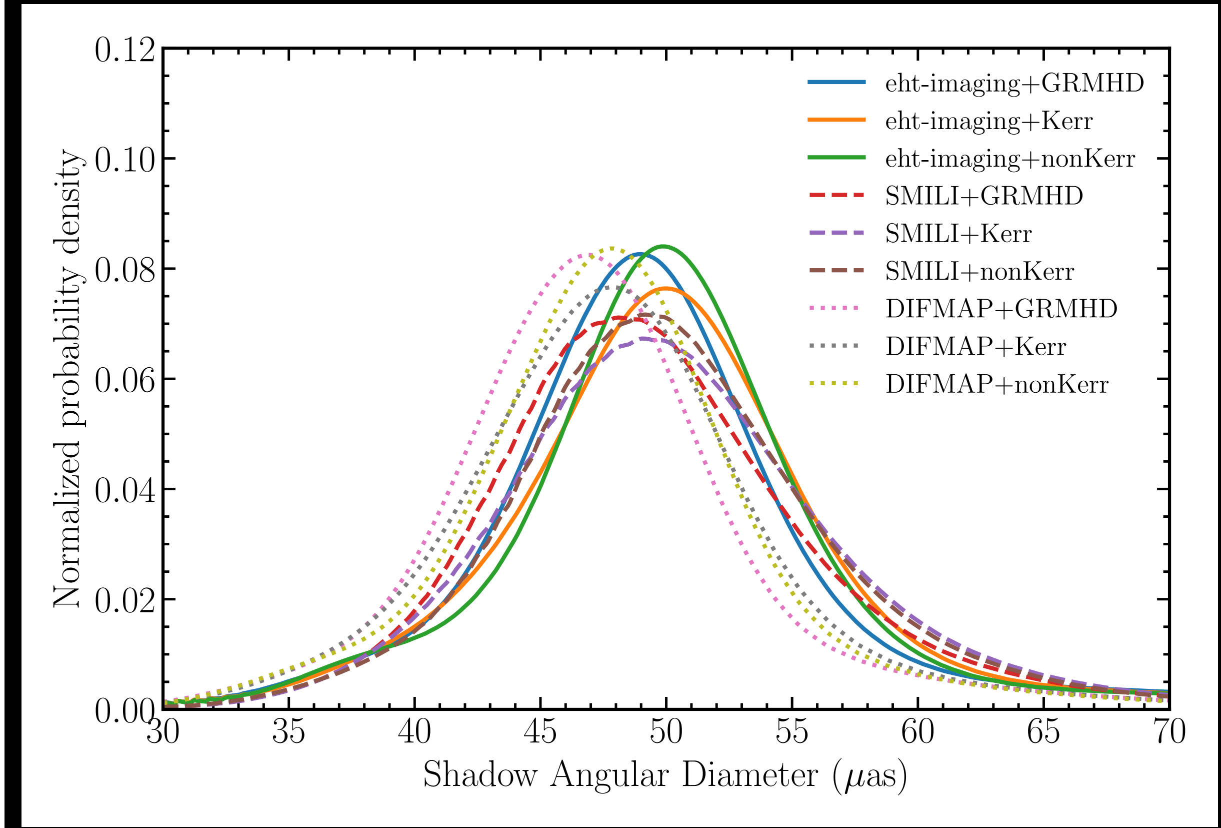

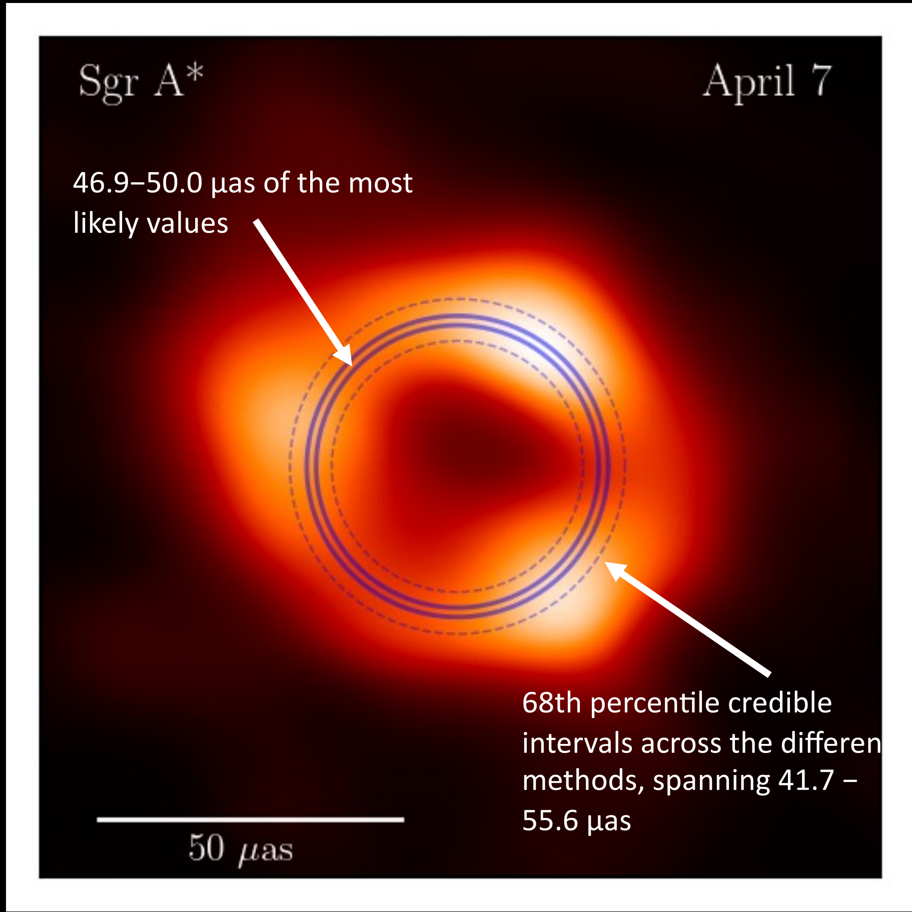

- Solid line shows the range of most likely values
- Dashed lines show the envelope of the 68th percentile credible interval for all methods

Inferred diameter of the black hole shadow boundary overlaid on the average EHT image of Sgr A∗ obtained from the 2017 April 7 data

Imposing constraints on the metric parameters of non-Kerr spacetimes

We used the priors on the mass-to- distance ratio to place constraints on metrics that are parametrically different from Kerr as well as on charges of several known spacetime solutions.

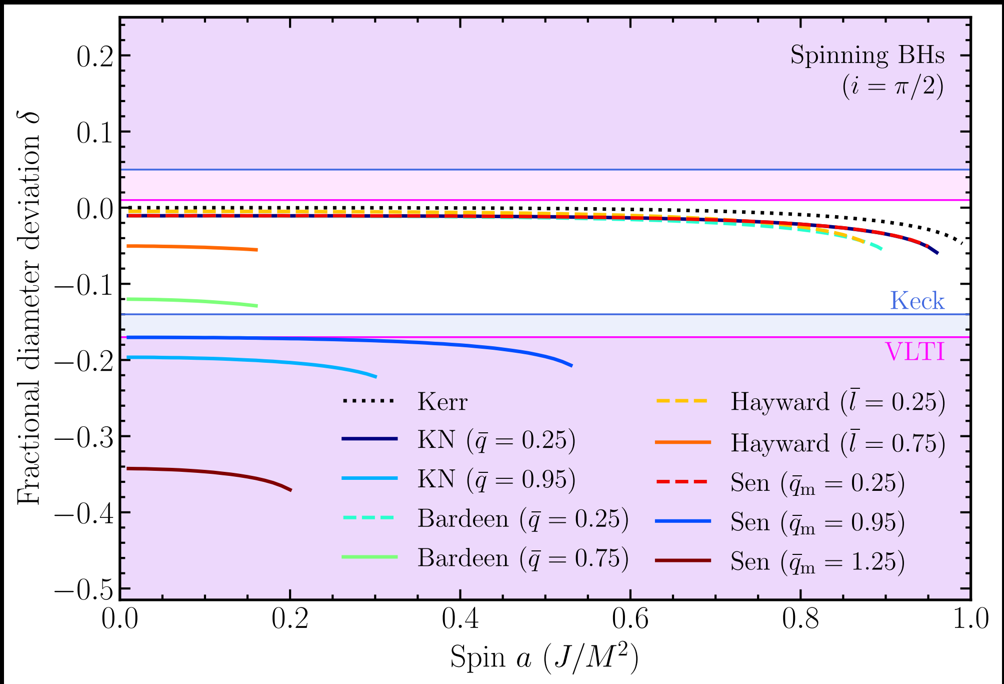

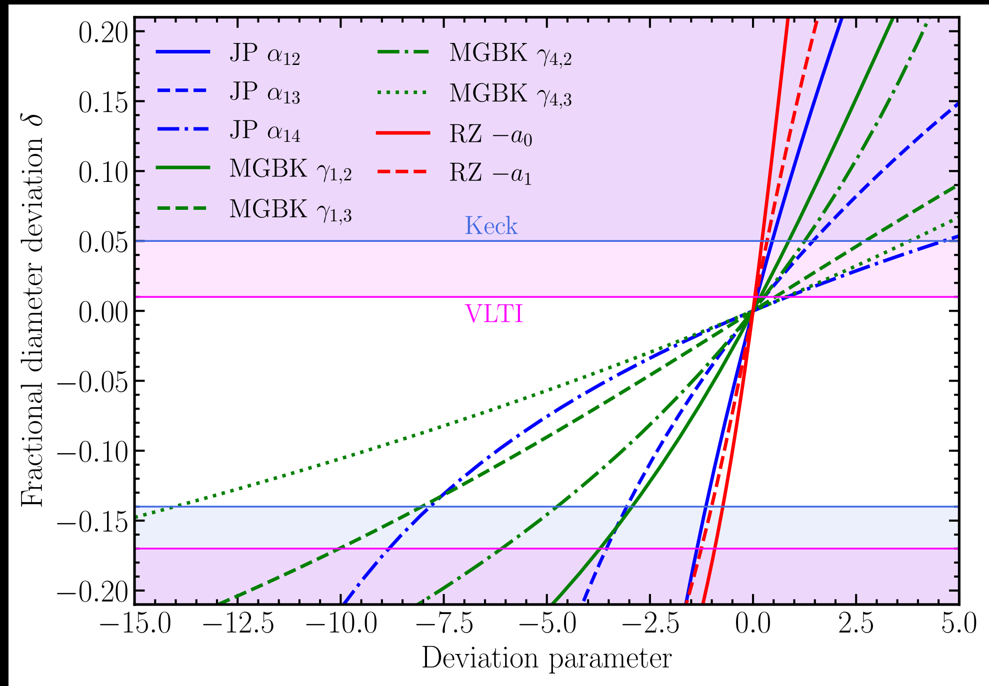

The white regions correspond to shadow sizes that are consistent at the 68% level with the 2017 EHT observations for Sgr A*

The regions excluded by the Sgr A* constraints using Keck (VLTI) are shown in blue (magenta)

M87 Imaging Tests

- M87 is 1500 times more massive than Sgr A*.
- Both black holes' images probe similar potentials but different curvatures.
- Sgr A* had a precise mass-to-distance ratio from S0-2 star orbit;
- M87 had two priors, yielding small deviations
- Uncertainties in Sgr A* were smaller, resulting in half the deviation parameter bounds compared to M87.
- Both black holes' shadows align with the Kerr predictions despite size and mass differences.
- This supports the prediction of GR that black hole properties scale with their mass.

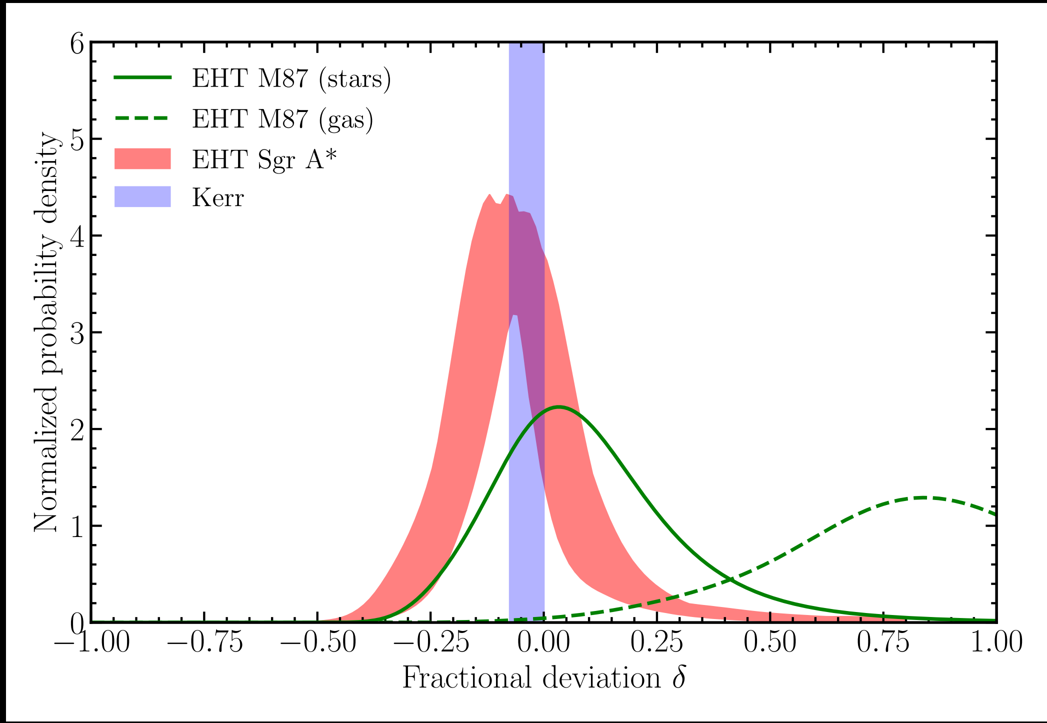

Comparison of the posterior distributions for the fractional deviation δ from the Schwarzschild predictions, as inferred by the EHT measurement of the size of the black hole shadows in Sgr A* and M87.

Gravitational-wave Tests

We compare the results on the deviation parameter for the two most constraining gravitational-wave events, GW170608 and GW190924, to those obtained for Sgr A*, as well as those for the M87 black hole.

In conjunction with the bounds found for stellar mass black holes and the one in the center of M87, our observations provide further support that the external spacetimes of all black holes are described by the Kerr metric, independent of their mass.

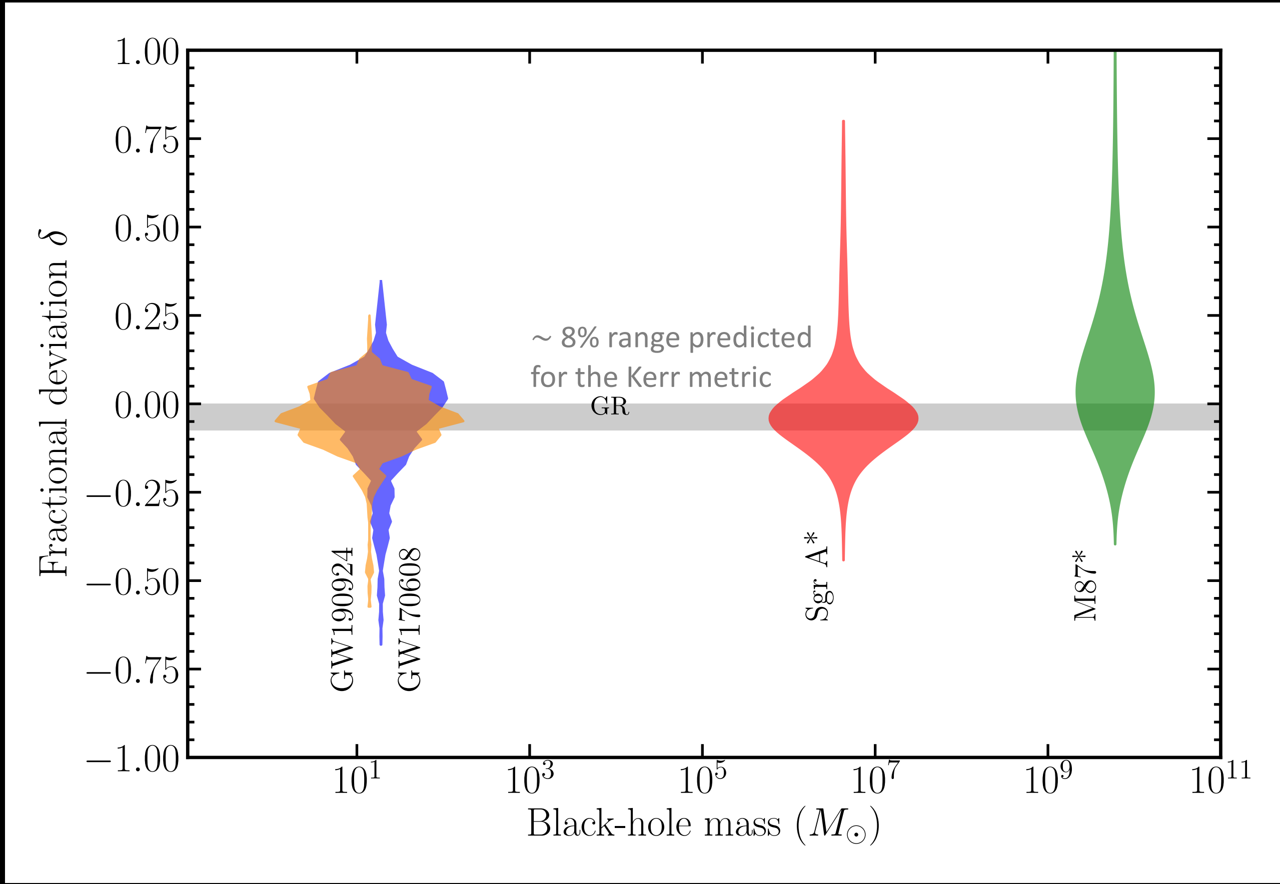

Take away points

- Images of Sgr A* probe a unique, not previously explored region of the parameter space of gravitational tests.
- Contrary to the case of M87, the Keplerian mass of Sgr A* is unambiguous, so there is no wiggle room in testing the predictions of the Kerr metric.
- Despite the vastly different masses, accretion rates, etc., the image sizes in both M87 and Sgr A* agree with the predictions of the Kerr metric.

Next Steps

Large distances

- Repeat the analysis once the GRAVITY data will be publicly available to confirm and improve our constraints

- Investigate the impact of closer stars, which are expected to probe the geometry of spacetime more efficiently.
  R. Della Monica, I. De Martino, M. De Laurentis, MNRAS 524, 3782 (2023)

- Investigate rotating metrics to forecast the future capability of GRAVITY data.

A Search for Pulsars around Sgr A* in the First EHT Dataset , P. Torne, R. Eathog, J. Wong,J.Cordes, M. De Laurentis, M. Kramer et al. ApJ 2023

Next Steps

Large distances

- Repeat the analysis once the GRAVITY data will be publicly available to confirm and improve our constraints

- Investigate the impact of closer stars, which are expected to probe the geometry of spacetime more efficiently.
  R. Della Monica, I. De Martino, M. De Laurentis, MNRAS 524, 3782 (2023)

- Investigate rotating metrics to forecast the future capability of GRAVITY data.

A Search for Pulsars around Sgr A* in the First EHT Dataset , P. Torne, R. Eathog, J. Wong,J.Cordes, M. De Laurentis, M. Kramer et al. ApJ 2023

Shed light on the underlying theory of gravity, the intrinsic nature of the SMBH in the Galactic center.

Short distances

- Better image fidelity and time-sampled "movies" of black holes.
- improved data from 2018, 2021, and 2022
- Additional telescopes included
- Higher frequency observations (345 GHz) provide 1.5x better resolution